Clemens Tschernay, BSc

Automatic Peak Finder:
A Tool to Find Diffraction Peaks in
Grazing Incidence X-Ray Diffraction Data

MASTER'S THESIS

to achieve the university degree of

Diplom-Ingenieur

Master's degree programme: Advanced Materials Science

submitted to

Graz University of Technology

Supervisor

Ao.Univ.-Prof. Dipl.-Ing. Dr.techn. Roland Resel

Institut für Festkörperphysik

Graz, March 2020

AFFIDAVIT

I declare that I have authored this thesis independently, that I have not used other than the declared sources/resources, and that I have explicitly indicated all material which has been quoted either literally or by content from the sources used. The text document uploaded to TUGRAZonline is identical to the present master's thesis.

_____
Date

_____
Signature

Acknowledgment

First of all I want to thank my family and my girlfriend Melanie Moser for their unconditional support. I am also very grateful to all my work group members, consisting of Verena Esslbauer, Benedikt Schrode, Sebastian Hofer, Lukas Legenstein, Manuel Kainz and Wolfgang Bodlos for their support during the creation and debugging of my program. I also want to thank some former members of my work group, Johanna Unterkofler, Jacopo Remondina und Andreas Hofer for enlightening discussions during the creation of the program.

I am especially grateful to Bendedikt Schrode, for all of his support at the times I had troubles with my code or GIDVis. He also shared his seemingly never-ending knowledge of data evaluation for grazing incident X-Ray diffraction. He also supplied my with data sets to test my code like the manual searches shown in the example section.

I am also very thankful towards Professor Roland Resel for the super introduction into the scientific world. Particularity, that he offered me the outstanding opportunity to conduct my measurements on the KAP crystal at the Synchrotron ELETTRA in Triest. This was an experience that I personally will always remember.

At last I want to thank Melanie Moser and Lisa Nais to proofreading my thesis.

Abstract

Automatic Peak Finder:
A tool to find diffraction peaks in
Grazing Incidence X-Ray Diffraction data

Clemens Tschernay

Institute of Solid State Physics, Graz University of Technology

Grazing Incident X-Ray Diffraction (GIXD) is a widely used tool to analyse crystalline thin films. For the evaluation of GIXD data the position of the diffraction spots is of great importance. So an accurate procedure to find diffraction peaks with their exact position is of utmost interest. In this thesis a specific procedure for peak finding is introduced and the software *Automatic Peak Finder (APF)* is developed. To begin with the search procedure of the *APF* looks for potential peaks. A potential peak must be a local maximum. The peak must not be located in an excluded area and must follow : (Intensity of experiment)-(Intensity of background) $\geq \sqrt{Intensity\ of\ background} * U$. Around these potential peaks boxes are drawn. Inside these boxes a two dimensional Gaussian fit is performed to get peak positions. If the peak is dismissed as a peak, although it can be clearly seen that a peak is present. An option for manual refinement of the boxes exist. For static GIXD only two elements of the scattering vector ($\vec{q} = (q_x, q_y, q_z)$) are determined. This two elements are q_{xy} ($q_{xy}^2 = q_x^2 + q_y^2$) and q_z. For rotating GIXD it is possible to get all three elements ($q_x, q_y and q_z$) of the scattering vector. The procedure is introduced on a number of examples: epitaxially grown molecular crystals at single crystalline surfaces (pentacenequinone on silver (111) and sexithiophene on potassium-chloride (100)) and a plate like potassium hydrogenphthalate crystal on a silicon wafer.

Kurzfassung

Automatic Peak Finder:
Ein Werkzeug zur Suche von Rögtenbeugungspeaks in Beugungsexperimenten mit streifenden Einfall.

Clemens Tschernay
Institut für Festkörperphysik, Technische Universität Graz

Grazing Incident X-Ray Diffraction (GIXD) ist ein weit verbreitetes Werkzeug zur Analyse kristalliner Dünnfilme. Für die Auswertung von GIXD-Daten ist die Position der Beugungspunkte von großer Bedeutung. Daher ist ein genaues Verfahren zum Auffinden von Beugungspeaks mit ihrer genauen Position von höchstem Interesse. In dieser Arbeit wird ein spezielles Verfahren zur Peakfindung vorgestellt und die Software *Automatic Peak Finder (APF)* entwickelt. In einem ersten Schritt sucht die Suchprozedur von *APF* nach möglichen Spitzen. Ein potentieller Peak muss ein lokales Maximum sein. Der Peak darf sich nicht in einem ausgeschlossenen Bereich befinden und muss folgen: $I_{Experiment} - I_{Hintergrund} \geq \sqrt{I_{Hintergrund} * U}$. Um diese potenziellen Spitzen herum werden Rechtecke gezeichnet. Innerhalb dieser Rechtecke wird eine zweidimensionale gaußscher Fit durchgeführt, um Spitzenpositionen zu erhalten. Wenn der Peak als Peak ignoriert wird, obwohl deutlich zu sehen ist, dass ein Peak vorhanden ist. Es besteht eine Option zur manuellen Verfeinerung der Boxen. Für statisches GIXD werden die beiden Elemente des Streuungsvektors ($\vec{q} = (q_x, q_y, q_z)$) bestimmt. Diese beiden Elemente sind q_{xy} ($q_{xy}^2 = q_x^2 + q_y^2$) und q_z. Für rotierendes GIXD ist es möglich, alle Elemente des Streuungsvektors zu erhalten. Das Verfahren wird an einer Reihe von Beispielen vorgestellt: epitaktisch gewachsene Molekülkristalle an einkristallinen Oberflächen (Pentacenchinon auf Silber (111) und Sexithiophen auf Kaliumchlorid (100)) und ein flacher scheibenähnlicher Kaliumhydrogenphthalatkristall auf einem Siliziumwafer.

Contents

1 Introduction

X-rays are electromagnetic waves with short wavelengths ($\sim$0.1 nm). Due to their electromagnetic behaviour the waves interact with the electron densities of matter. Today, X-rays diffraction experiments are standard techniques to determine crystalline properties of materials. Typically, X-ray diffraction is applied to organic single crystals (e.g. protein crystals) or bulk materials. Also thin films can be investigated by X-Ray diffraction techniques. [8]

A crystal structure is a periodical arrangement of building parts of the crystal. These parts can be in the simple cases atoms or in case of molecular crystals even a (ordered) molecule film.

The crystal structure can be determined experimentally by first measuring the scattering vector $\vec{q}$. To interpret these experiments, the famous Laue equation is used.[8] The Laue equation gives the relation of the reciprocal lattice vector :

$$\vec{G}_{hkl} = \vec{q} \tag{1.1}$$

where: $\vec{q}$...scattering vector.
          $\vec{G}_{hkl}$...reciprocal lattice vector.

The reciprocal lattice vector is defined as:

$$\vec{G}_{hkl} = h\vec{a}^* + k\vec{b}^* + l\vec{c}^* \tag{1.2}$$

where: the hkl values are the Laue indices.
               $\vec{a}^*, \vec{b}^*, \vec{c}^*$ are the reciprocal lattice vectors.

With this information the unit cell parameters can be determined. During this step the peaks can also be assigned to a specific crystal plane.[16] [15]

2 Fundamentals

2.1 X-Ray Diffraction (XRD)

In XRD measurements an incident beam, with the wave vector $\vec{k}_{in}$, hits a sample with the incident angle α_i and is diffracted. The diffracted beam, with a wave vector $\vec{k}_{out}$, then hits a X-ray detector. The measurement parameter is the amount of detected X-rays, labelled as intensity in counts. To calculate the scattering vector $\vec{q}$, the definition of the scattering vector 2.1 is used [2]. This is only valid as long as elastic scattering occurs, which means that: $\left|\vec{k}_{in}\right| = \left|\vec{k}_{out}\right|$

$$\vec{q} = \vec{k}_{out} - \vec{k}_{in} \tag{2.1}$$

The elements of the scattering vector are:

$$\vec{q} = \begin{pmatrix} q_x \\ q_y \\ q_z \end{pmatrix}$$

When the Laue equation (1.1) is fulfilled Bragg peaks can occur, as long as $\vec{k}_{in}$ is co-planar to $\vec{k}_{out}$. If the incident angle has the same angle as the angle from the wave vector to the sample, the measurement is called a "Specular scan". The information obtained from this scan is $\vec{q} = q_z$. With this technique information of the out-of-plane orientation can be determined.[8].
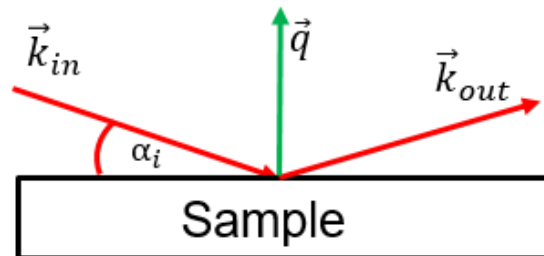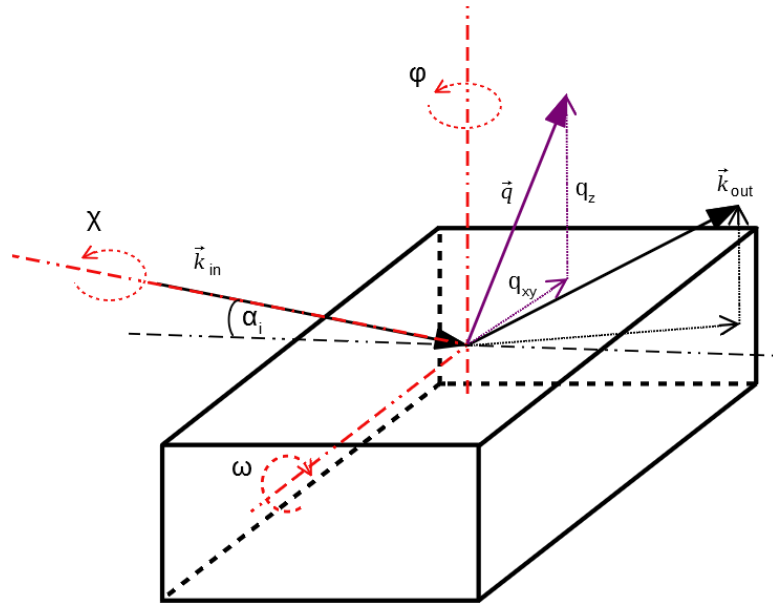

Figure 2.1: A sketch of an X-ray diffraction measurement. $\vec{k}_{in}$ is the incoming wave vector. The wave vector hits . $\vec{k}_{out}$ is the diffracted wave vector. $\vec{q}$ is the scattering vector.

### 2.1.1 Grazing Incidence X-Ray Diffraction (GIXD)

Grazing Incident X-Ray Diffraction(GIXD or GIXRD) is a special case of XRD, where the incident angle α_i is the regime of total external reflection. A sketch can be seen in Figure 2.2. This allows the beam to be surface sensitive and thus be able to collect data from thin films. The drawback of this measurement set up is that the footprint (illuminated area) of the sample is relatively large.[8]

Figure 2.2: A sketch of an X-ray diffraction measurement in a grazing incident setup. $\vec{k}_{in}$ is the incoming wave vector. $\vec{k}_{out}$ is the diffracted wave vector. $\vec{q}$ is the scattering vector, with the components (dotted magenta line) q_{xy} and q_z. α_i the incident angle, ϕ the rotation axis of the sample, ω and χ rotations around axes (red point dashed lines) further described in section 2.5. The dotted black lines are 2 components of $\vec{k}_{out}$ to show change of the paths (by black dot dashed line) Figure is based on [16]

The accessible volume of the reciprocal space is limited to the wavelength λ. An example of this can be seen in Figure 2.3a. The blue area consists two half circles with the radius of $|\vec{q}| = \frac{2\pi}{\lambda}$. Hereby, λ is the wavelength of the X-ray beam . A three dimensional diagram of the accessible volume for GIXD can be seen. In this diagram $\lambda = 1.4$ Å . The "Specular scan" mentioned in section (2.1) is visible as a green line in this figure. The red half circle has a radius of $|\vec{q}| = \frac{4\pi}{\lambda}$. Within this area several other X-ray diffraction techniques (e.g. rocking curve measurements) can be performed. [8]. In Figure 2.3a there is also a dashed magenta half circle. This line symbolises a Debby-Scherrer rings, which will occur when there are randomly oriented crystallites within the sample. These rings have a defined $|\vec{q}|$ value. In Figure 2.3b a three-dimensional model of the accessible reciprocal space with a GIXD measurement with wavelength $\lambda = 1.4$ Å is shown.

Depending on the in-plane order of the thin film crystallites on the sample, there are two possibilities of GIXD, which can be applied: "static GIXD" and "rotating GIXD"
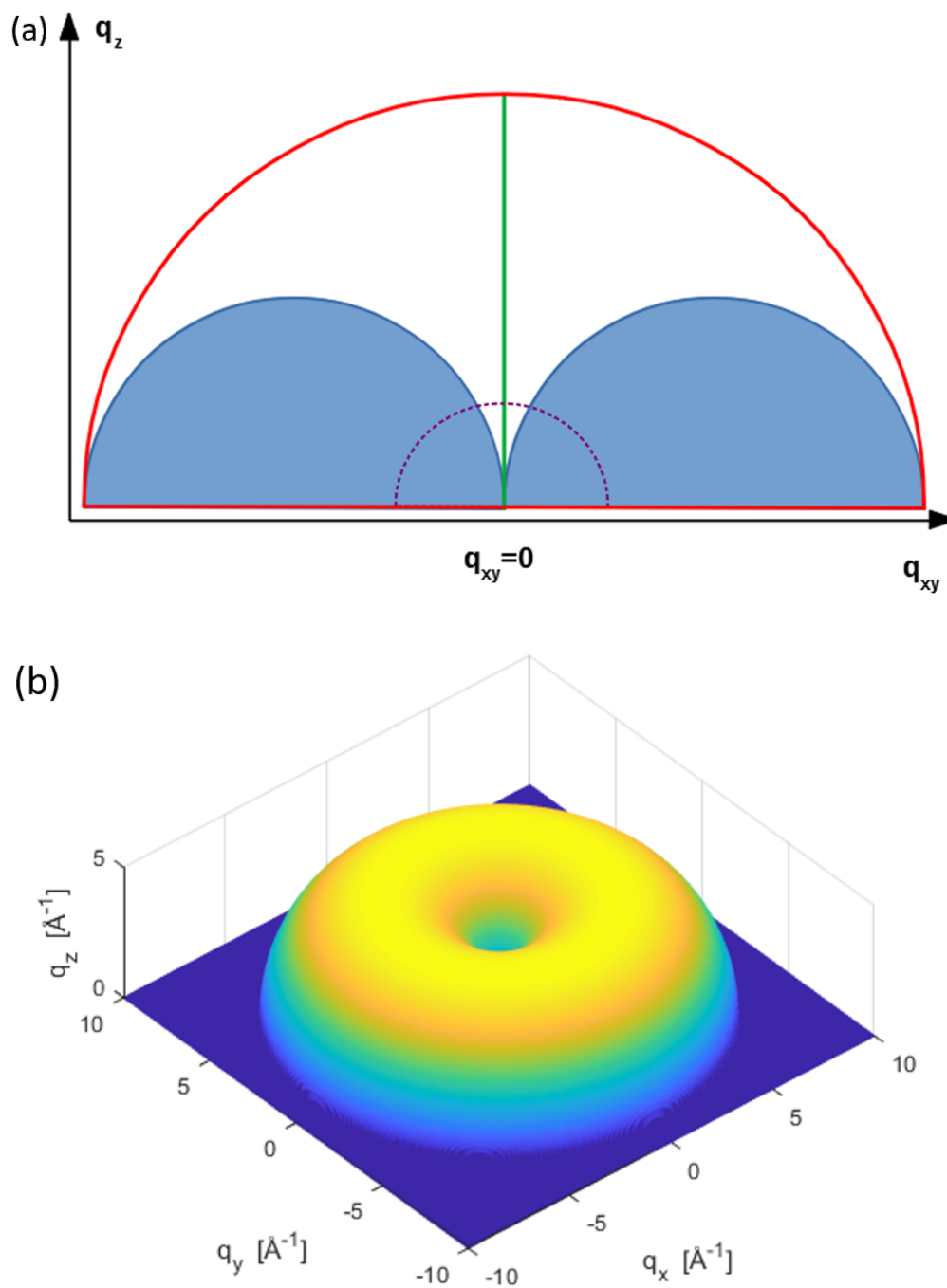
Figure 2.3: (a) This sketch represents the reciprocal space. The coloured lines and areas are the measured areas in different X-ray diffraction methods. **Blue areas**: measurable with GIXD; **green line**: area of a "Specular scan"; **magenta line**: a Debye-Scherer ring; **red half circle**: with rocking curves points within this area can be deduced. This figure is also based on [8]. (b) shows the volume available in grazing incident X-ray diffraction.
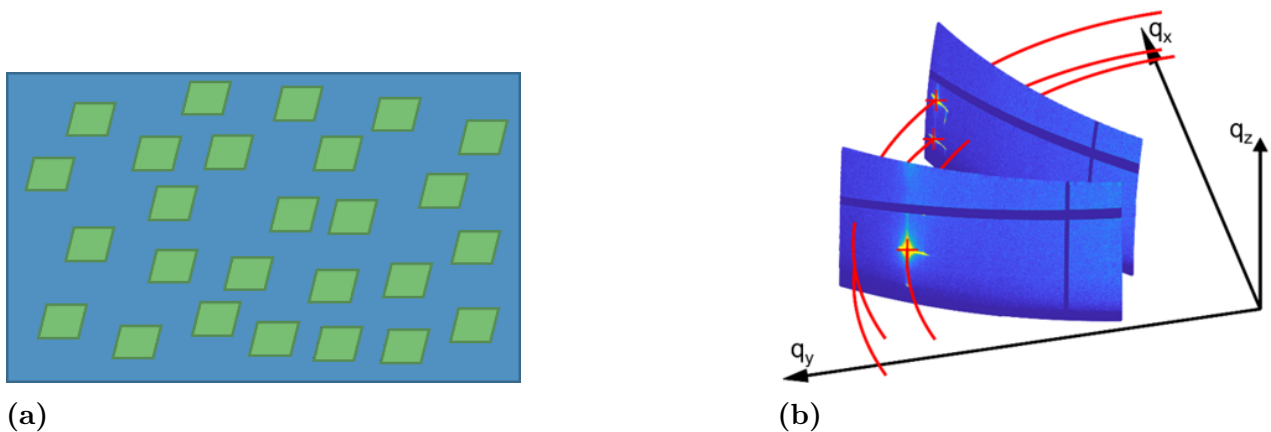
Static Grazing Incident X-Ray Diffraction

In static GIXD the sample is kept in its place and is not moved in any direction during the experiment. This is done for samples with no preferred in-plane alignments. For these samples the reciprocal lattice points G_x and G_y will scatter around a circle and thus are not distinguishable in the measurements. An example for static GIXD crystals and their pattern can be seen in Figure 2.4.

(a)

(b)
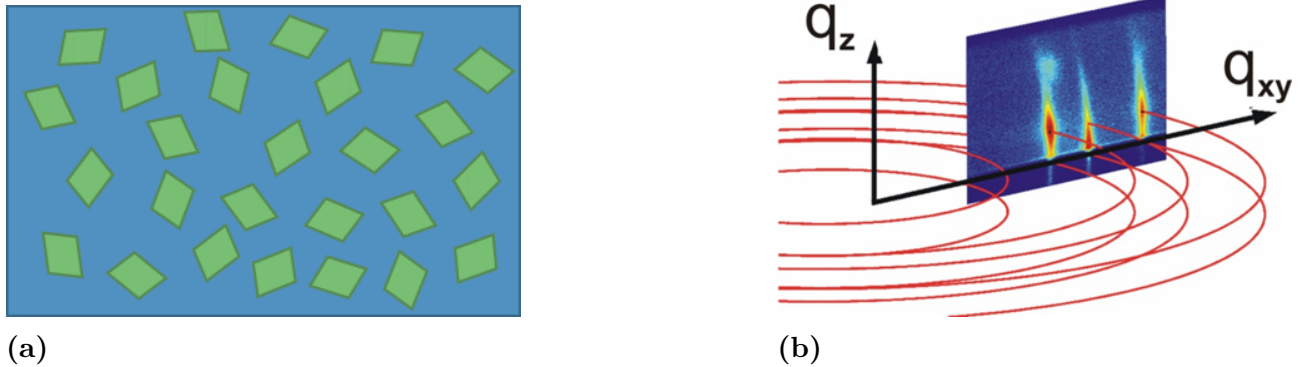
Figure 2.4: (a) Crystallites with no in-plane alignment [11] (b) Example measurement patter of the grazing incident X-ray diffraction experiment.[10]

Rotating Grazing Incident X-Ray Diffraction

When the sample is rotated during the measurement, this method is called rotating grazing incident X-ray diffraction. With this technique samples with good in-plane orientation can be measured. The measurement of the diffraction pattern is performed, as an integration during a rotation of the sample over a defined number of degree ($\Delta\phi$). This measurement is performed multiple times until a 360° rotation of the sample is performed. Ways to treated this datasets, are discussed in section 2.5.1. Figure 2.5a shows an in-plane aligned sample. This type of sample needs rotating GIXD to be measured, because the in-plane alignment diffraction peak occurs only at specific rotation angles. This is noted with red crosses in Figure 2.5b. In this picture the red circles are just markings of a specific angle, so that it can be seen that the peaks are not always visible. [5]


(a)

(b)

Figure 2.5: (a) Crystalites with perfect in-plane alignment [11] (b) Two diffraction patterns of rotating grazing incident X-ray diffraction measurement data. At the spots marked with a red x the peaks are marked at the measurement. [12]

2.2 Single versus Thin Film Diffraction Experiments

In Figure 2.6 two diffraction patterns are shown. In Figure 2.6(a) a pattern of a single crystal diffraction pattern can be seen. There are many peaks which have a strong intensity compared to the background. There are different geometries for single crystal diffraction experiments. A well known example is a four-circle Eulerian goniometer[1]. The automated evaluation of single crystal diffraction data is today also standard. An example for a software for evaluation of single crystal diffraction patterns is called XDS[6].

On the right hand side, there can be seen a diffraction pattern of Pentacenequinone crystals on a Ag (111) surface. Two types of peaks can be seen: The strong peaks of the silver (111) surface on the right and polycrystalline silver can bee seen as ring-like structures. The second peak type is generated by the thin film. This peaks are located in the middle of the diffraction pattern. The thin film peaks are significantly weaker than the silver peaks. Some of them are so weak that they are barely distinguished from the background. The reason for the dark blue lines is discussed in section 2.3.1.

(a)

(b)
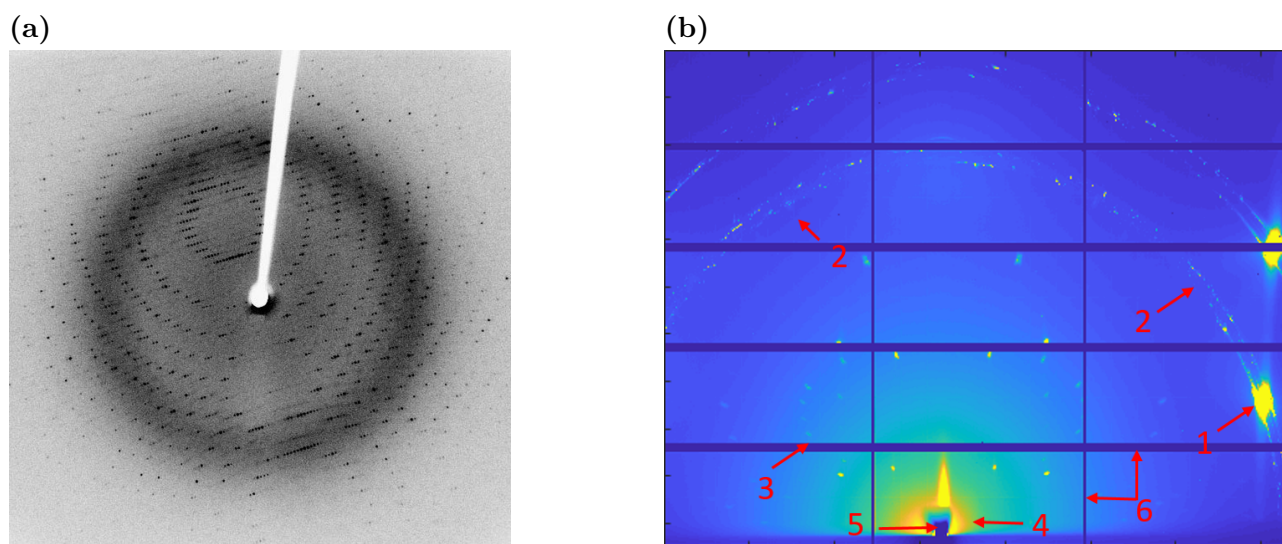
Figure 2.6: (a) A single crystal diffraction pattern.[3] (b) The measurement of a Pentacenequinone thin film on a Ag (111) surface. **1**: substrate peaks, **2**: polycrystalline substrate peaks, **3**: thin film peaks, **4**: air scattering, **5**: shadow of beam-stopper, **6**: detector properties

2.3 X-Ray detection

This section is designed as a brief introduction. For further information on X-Ray detectors see [1]. There are three different methods. The oldest detection technique uses photoactive films. The more X-rays hit the film, the stronger the peaks are. Later on techniques to count single X-Ray are introduced. Then, there is also a combination of this two methods exists, called Area detectors or hybrid detectors.

2.3.1 Detector properties of Pilatus 2M

During the experiments at the synchrotron ELETTRA Trieste, a Dectris Pilatus 2M detector was used. The detector is a two dimensional hybrid detector (combination of area and series detector), which is built up by 8 x 3 single Pilatus detector modules. Each of these modules consists of a layer of silicon sensing chips. This chips are then connected to a series of read out chips, which are then connected to a electric readout circle. To prevent dirt or light damaging the detector on the front side of the detector is protected by a Mylar foil. For further information see [7]. The module style of the Pilatus 2M has an influence on the measurements. Between modules there are a short areas, were no measurements can be performed. The given output file of the detector just leaves these areas with a predefined value (depending on the data format). At the edges of these modules higher intensities than expected will occur. Following a closer investigation of the detecotr, the modules have higher intesities at specific positions than expected. These areas have to be ignored in the data sets. To ignore this false data a matrix called 'AREA_OF_DETECT_BAD' has to be created. In this matrix, which has to be of the same size as the detector pictures, is 0 at all untrusted areas and 1 on all trusted areas.

The array of Pilatus modules also has an influence on the experimental set up. The centre pixel (the pixel on which the reflected beam would hit the sample) must not be located in the middle of the detector. To understand this it is important to know that the same diffraction spots will occur on the left and the right side of the detector in rotating GIXD. This means the data is symmetrical to the $q_z = 0 \text{Å}^{-1}$ line. In order not to lose any peaks the centre pixel is shifted outside the centre of the detector. Otherwise both peaks could be located in a module gap.

| Properties	Value
Pixel Size	172 x 172 μm^2
Point-spread function	1 pixel
Format	1475 x 1679 = 2476525 pixels
Intermodule gap	x: 7 pixels, y: 17 pixels, equals: 8.0% of total area
Readout time	3.6 ms (frame rate 30 Hz)
Adjustable threshold	range 2- 20 keV (energy resolution 500 eV)
Energy range	3 - 30 keV (quantum efficiency: 3 keV 80%; 8 keV 99%; 15 keV 55%)
Counting rate per pixel	$> 2 \text{ x } 10^6 Photons/s$
Data Formats	CBF (mosflm, xds); TIF (fit2d, AreaDiffractionMachine)

Table 2.1: Properties of Pilatus 2M in the measurements. For full list see: Website of ELETTRA [9].

2.4 Experiment

The grazing incident diffraction experiments (as described in section 2.1.1) used in this thesis were performed at the synchrotron ELETTRA, Trieste at the XRD1 beamline. The measured parameters is the intensity in counts per pixel. This intensity is collected as a two dimensional data.

2.4.1 Experimental Setup

In Figure 2.7 a top view of the measurement setup is shown. On the right side, the used Pilatus 2M detector from Dectris can be seen(4). In the middle, the vacuum sample holder (2) can be seen. This sample holder can rotate around 360°. Between the sample stage and the detector the beam-stopper (3) can be seen. The beam-stopper is put in the path of primary beam reflection to prevent damaging the detector. On the left side of the sample stage, the insertion nozzle (1) can be seen. For setup parameters see also the webpage of ELLETRA about the XRD1 beamline [9].
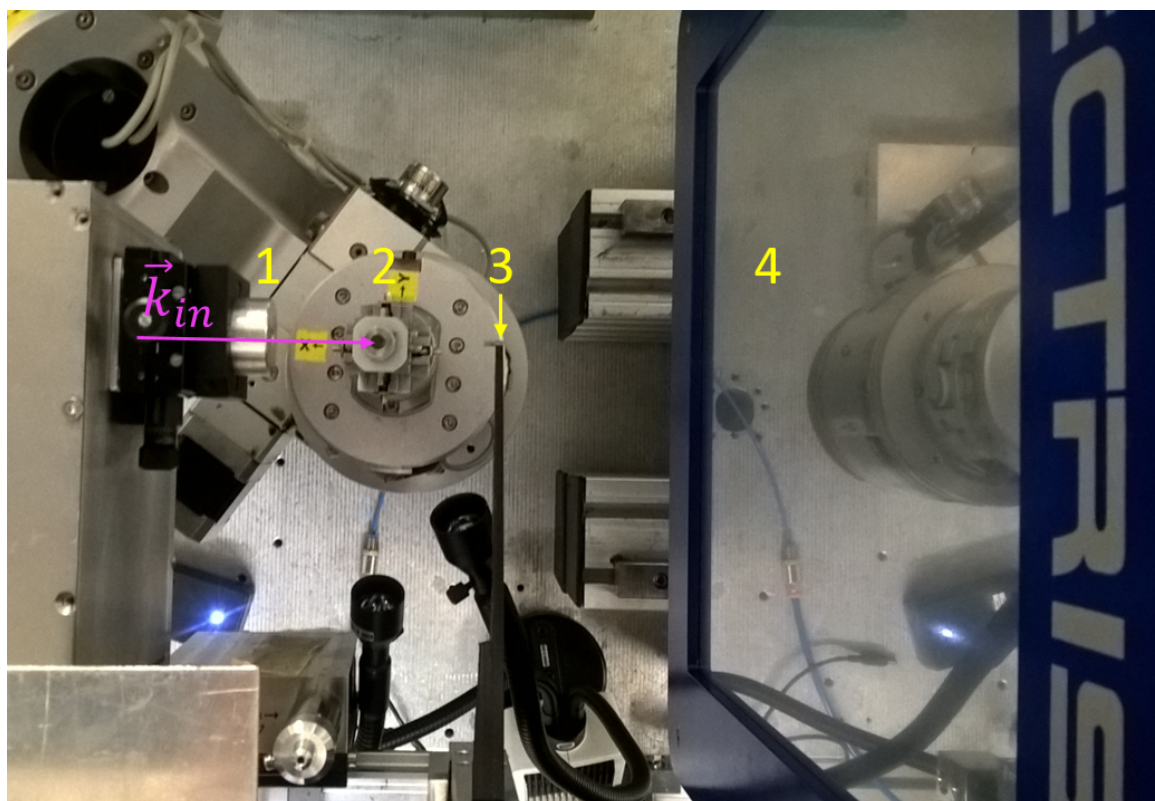

Figure 2.7: Top view of the measurement setup of the XRD1 beamline at the synchrotron ELETTRA.[11] **1**: Nozzle where the beam (pink arrow) enters the setup; **2**: sample stage with vacuum holder; **3**: beam-stopper; **4**: detector (Dectris, Pilatus 2M).

2.5 GIDVis - A Software for GIXD Evaluation

GIDVis is a software developed for the visualisation and evaluation of GIXD data. The structure of GIDVis is modular, which allows users to expand the software packages if needed. GIDVis can display the most common file formats, like .tiff, .cbf., etc. The data can be transformed to show the intensities in a reciprocal space. This option is called "Q-space", because the measured intensity of the scattering vector $\vec{q}$ is colour-coded and split into its q_{xy} and q_z elements(see Figure 2.8b). If the diffraction pattern is displayed in the option "Polar space", the data is shown as the length of the scattering vector $|\vec{q}| = \sqrt{q_{xy}^2 + q_z}$ and the angle $\Psi = atan(\frac{q_{xy}}{q_z})$(see Figure 2.8c). For the transformation into "Q-space" or "Polar space" the experimental values of (ω) a rotation around perpendicular to the primary beam and a tilt with the path of the primary beam as rotation axis (χ) are needed and have to be inputted manually into GIDVis. If $\chi = 0$, ω equals the incident angle.

It is also of utmost importance that a beamtime file is exists for the measurement session. In this beamtime file, parameters like the size of the detector in pixels, the sample detector distance, the position of the centre pixel and the wavelength of the X-Ray beam (λ), etc. To create such a file a calibration measurement (e.g. LaB_6 - Lanthanum hexaboride) has to be performed. Then, GIDVis offers the possibility of a calibration wizard, which helps to extract the parameters for the beamtime file. For more information on GIDVis see[12] or the GIDVis manual [10].
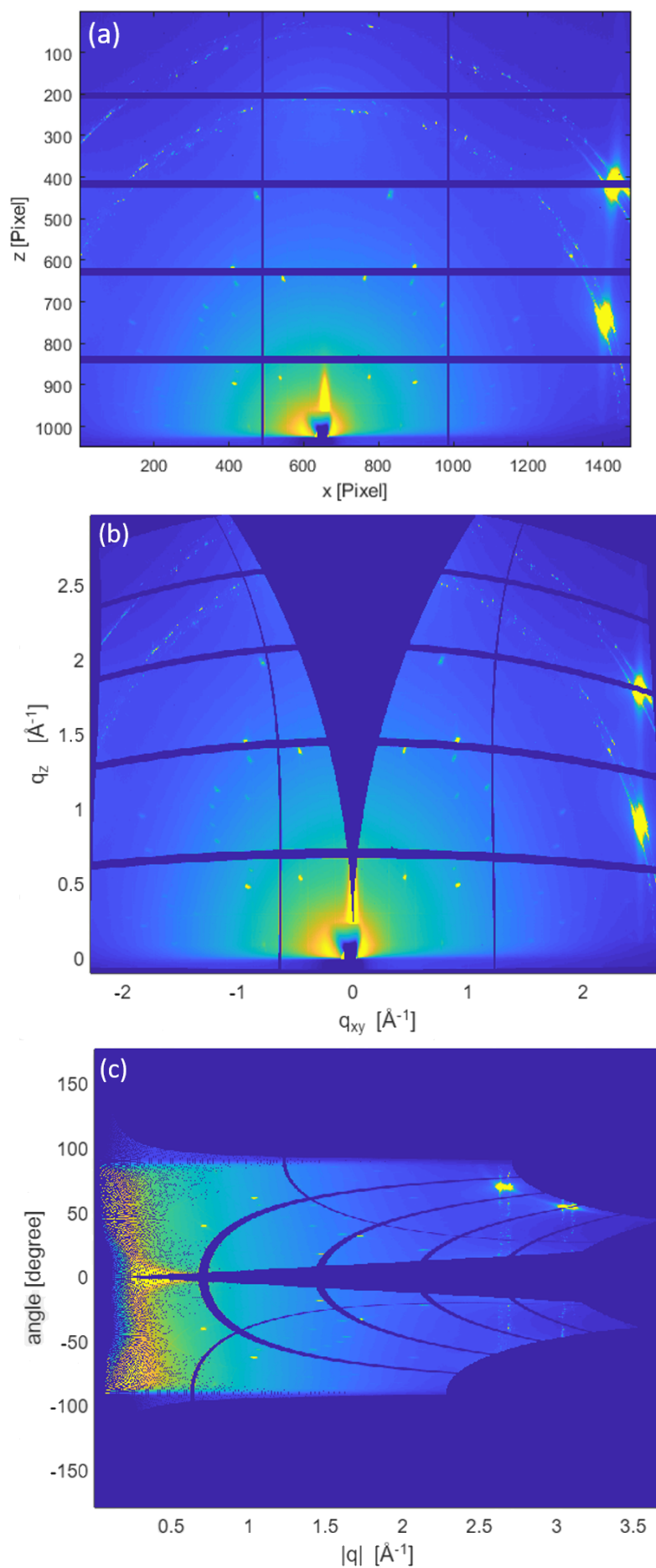
Figure 2.8: The different spaces available in GIDVis. (a) Data at the detector. (b) The "Q-Space". (c) The "Polar space".

2.5.1 Data representation for rotating GIXD

In case of rotating GIXD, multiple diffraction patterns are taken during the experiments. To display these data, GIDVis offers multiple possibilities. The three most useful options are: "Summed image", "Maximum intensity image" and "Multiple Scan plot".

Summed Image

This option shows the pixel-by-pixel summation of each diffraction pattern. This then leads to a single picture, depicted in Figure 2.9. In the "Summed Image" the strongest peaks (eg. substrate peaks) can be observed best. Peaks, which are not significantly higher than the background, are difficult to visualize. This is the case because the slightly higher peak will stand out less from the additionally summed up background (and its noise).
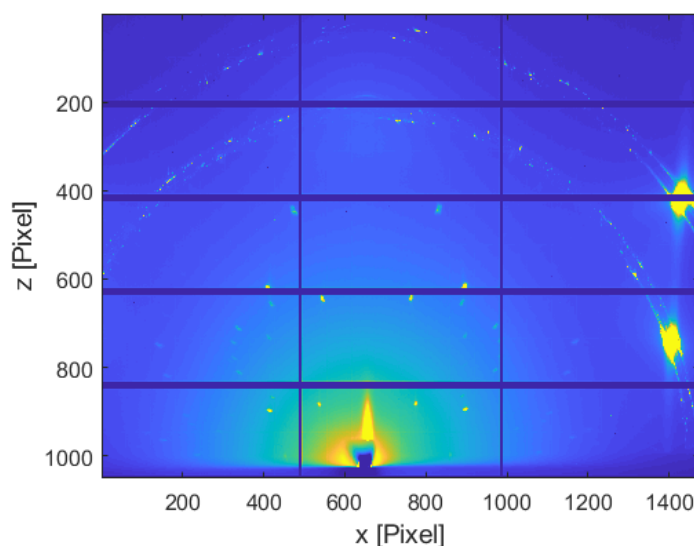
Figure 2.9: The "Summed Image" of a Pentacenequinone thin film on a Ag (111) surface. The strong peaks at x=1400 pixel and z=750 pixel and z=400 pixel are substrate peaks. Around x=650 pixel and z= 1000 pixel. The shadow of the beamstop and the air scattering around it can be observed. Peaks of the thin film can be seen in the area of x=300 to 1000 pixels and z=400 to 900 pixel.

Maximum Intensity Image

This mode uses the maximum intensity value of each pixel of the rotation pictures, which are plotted. An example of this can be seen in Figure 2.10. In this figure all features are clearly visible, because the maximum intensity of a peak is much higher than the intensity of the highest points of the background noise. Not only strong and weak peaks are visible, but also some unwanted features, such as the spurious intensities of the detector described in section 2.3.1. Also two Debye-Scherrer-like rings appear. These rings are fragments of little crystallites of the substrate with an orientation different from the (111) surface.
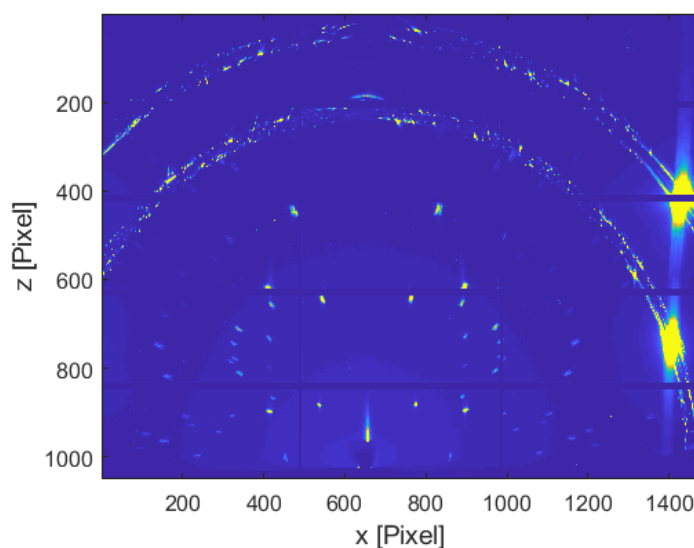
Figure 2.10: The "Maximum Intensities" of the diffraction patterns of a rotating GIXD experiment of a Pentacenequinone thin film on a Ag (111) surface. At x=1400 pixel and z=750 pixel and z=400 pixel the peaks of the substrate are visible. Peaks of the thin film can be seen in the area of x=300 to 1000 pixels and z=400 to 900 pixel.

Multiple Scan plot

In this option a specific area of the diffraction pattern is summed up. This is performed by using each diffraction pattern of the rotation. The intensity is then plotted over the number of pictures (N). An example of this can be seen in Figure 2.11. In this example it can be seen that the intensity changes considerably during the rotation. There are 12 peaks, which seem to form 6 groups of 2 peaks. For further explanation of this behaviour see section 3.4.1. From the number of pictures (N), the rotation angle ϕ_{sample} can be easily calculated: $\phi_{sample} = N \cdot \Delta\phi$. In this formula, $\Delta\phi$ is the step size over which the integration runs during the measurement. With this relation and the knowledge, in which picture the peaks are located, the q_{xy} component can be split into the q_x and q_y components.
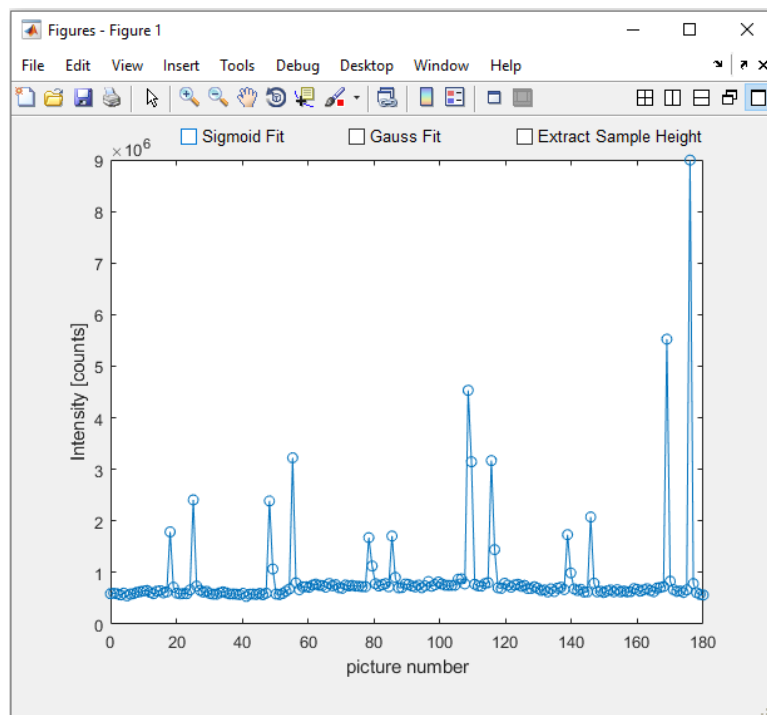
Figure 2.11: GIDVis window from the "Multiple Scan" plot. The used area to create this plot, is a boxlike area around a thin film peak. This peak can be observed in Figure 3.2 at q_{xy}=0.5 Å^{-1} and q_z=0.5 Å^{-1}.

3 Automatic Peak Finder

In this chapter of the *Automatic Peak Finder (APF)*, a module for GIDVis, will be described. In Figure 3.1 the graphical user interface (GUI) of the peak finder is explained. The GUI is split up in three parts. On the left side, an axes system is located, where the diffraction patterns are depicted. On the right, there are two tab groups. For searching the peaks the upper tab group is used. The values will be discussed during this chapter. The lower tab group is used for display settings axes system. For example, the colour-map and its colour limits can be set. Also, there are some other additional functions, like saving the current status of the GUI or loading an old status of the *APF*. These functions should be self-explanatory. An important annotation is that if the GUI is closed, the current status will be automatically saved in a file with the name "Settings.mat".
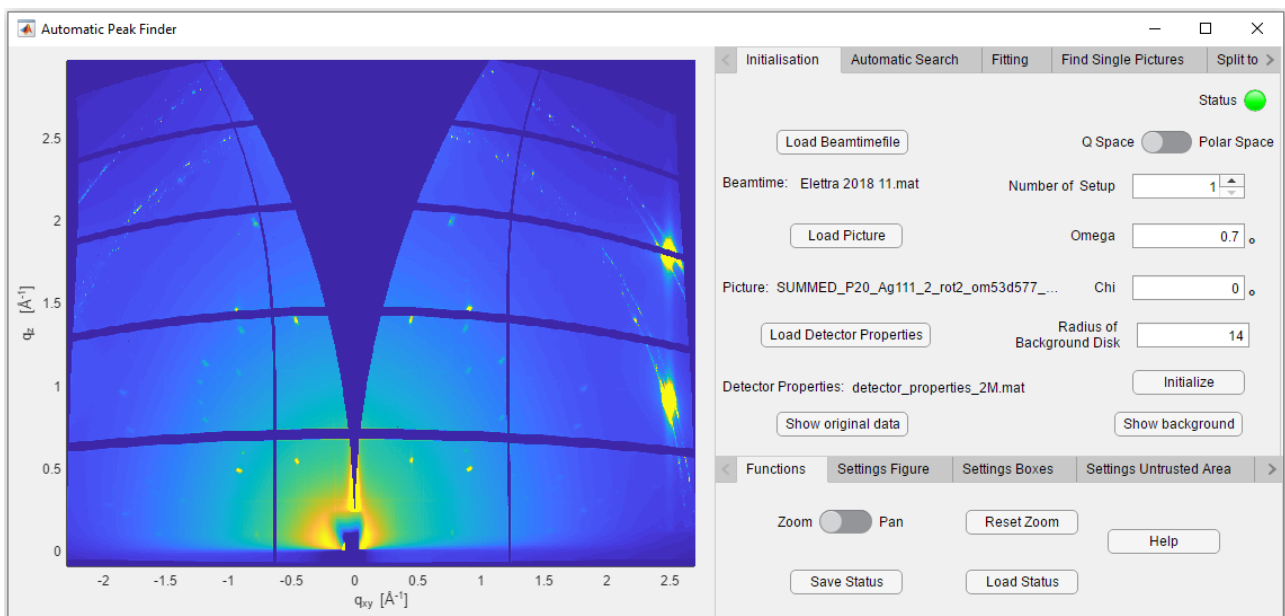
Figure 3.1: The graphical user interface of the *Automatic Peak Finder* after the initialization step. This interface consists of an axes area on the left, where the diffraction patterns are shown, and two input panels on the right. The lower tab group is used for display settings and additional Functions. The upper tab group is used for the input of required values for the search procedure.

3.0.1 Start up

There are two different start up modes: Start up with default settings or start up with previous settings. The default case happens, when the "Settings.mat" file is not existent. Then the *APF* starts with some default values (see table 3.1). A message box will inform the user about the default start up. If some previous settings exist, these settings from the automatic saved status are used. This process could take a while, so a message box is created at the beginning of the loading process and closed again after the start up is finished.

Parameter	Value	Unit
Switch	Q Space	
Number of Setup	1	
Omega	0	°
Chi	0	°
Radius of Background Disk	14	
Box height	0.05	Å^{-1}
Box width	0.05	Å^{-1}
Sensitivity start	28	
Sensitivity steps	50	
Sensitivity end	27	
Threshold sigma q_{xy} of static GIXD	0	Å^{-1}
Threshold sigma q_z of static GIXD	0	Å^{-1}
GoF of static GIXD	0.4	
Sensitivity	7.5	
Threshold sigma q_{xy} of rotating GIXD	0	Å^{-1}
Threshold sigma q_z of rotating GIXD	0	Å^{-1}
GoF of rotating GIXD	0.4	
caxis min	0	
caxis max	0	
Font Size	12	
Colourmap	parual	
Regridding Vertical Pixel	600	Pixel
Regridding Vertical Pixel	1200	Pixel
Linethickness of Boxes	0.5	
Colour of Boxes	green	
Linestyle of Boxes	-	
Colour of Untrusted Areas	red	
Linethickness of Untrusted Areas	0.5	
Linestyle of Untrusted Areas	-	
Thickness of Marker	5	
Colour of Markers	red	
Style of Marker Fit	+	
Style of Marker Q vector	o	

Table 3.1: The default values of the *Automatic Peak Finder*.

3.1 Initialization

Before the initialization step all the parameters of the experiment (diffraction pattern, ω, χ as defined in section 2.5) have to defined. Additionally required informations consists of the diffraction pattern and a "beamtime"(see section 2.5) file from GIDVis. To insert this files exist a button which opens a file selection user interface.[19]. "Number of Setup" is used to declare which setup of this beamtime file has to be used. A third file has to be loaded before the program can execute without an error message. This file has to contain a matrix called 'AREA_OF_DETECT_BAD'. This matrix has to have the same size as a matrix containing the detector pixels. 'AREA_OF_DETECT_BAD' is a logical matrix with 0 for all untrusted positions and 1 at all trusted positions. Additionally the radius of the Background disk(see section 3.1.1 for further information) has to be given. Also the user can specify if the data should be shown in terms of the q_{xy} and q_z elements or a polar space defined by these elements. The execution of the code starts when the user presses the 'Initialize' Button. During the following execution of the code a check is preformed if all the needed parameters are set. Then a background estimation is performed and the new diffraction pattern is displayed on the axis. There are also two possibilities to show the diffraction pattern at the detector ("Show original data") and the estimated background ("Show background") by clicking the corresponding buttons.
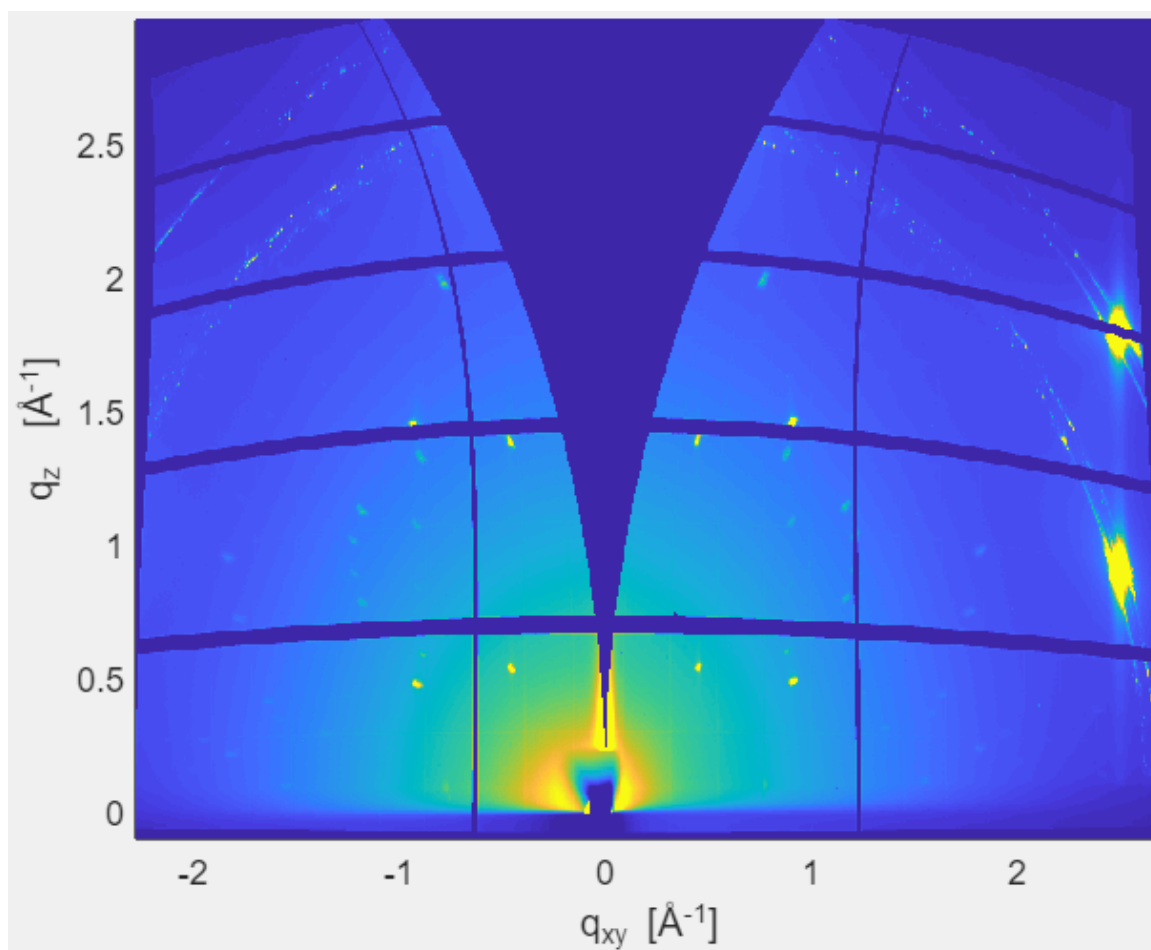
Figure 3.2: GIXD diffraction pattern of Pentacenequinone on a Ag(111) surface after the Initialization step. The pattern is shown in q space.

3.1.1 Background estimation

For the background estimation, a Matlab built-in function called *imopen*[18] is used. This function basically takes each pixel of the pictures and averages on a disk around that pixel. The radius of this disk can be defined by the user with the variable 'Radius of Background Disk'. The default radius is 14 pixel. In Figure 3.3 the steps of the background correction are visualized. In Figure 3.3a, the original data are shown. With these data, the background estimation described above is applied. The outcome is a blurry picture, which can be seen in Figure 3.3b. This picture is furthermore used as the new estimated background. The background is close to the centre pixel (the area where the reflection of the primary beam would hit detector) the highest. Surroundings of this area have a higher intensity due to air scattering. Further away of this centre pixel the background is lower. To see that this background can increase the contrast of our data, a subtraction form the original data is performed. This subtracted image is shown in Figure 3.3c. It can clearly be seen that all of the peaks are visible, but also the unwanted detector properties(discussed in section 2.3.1) are enhanced.
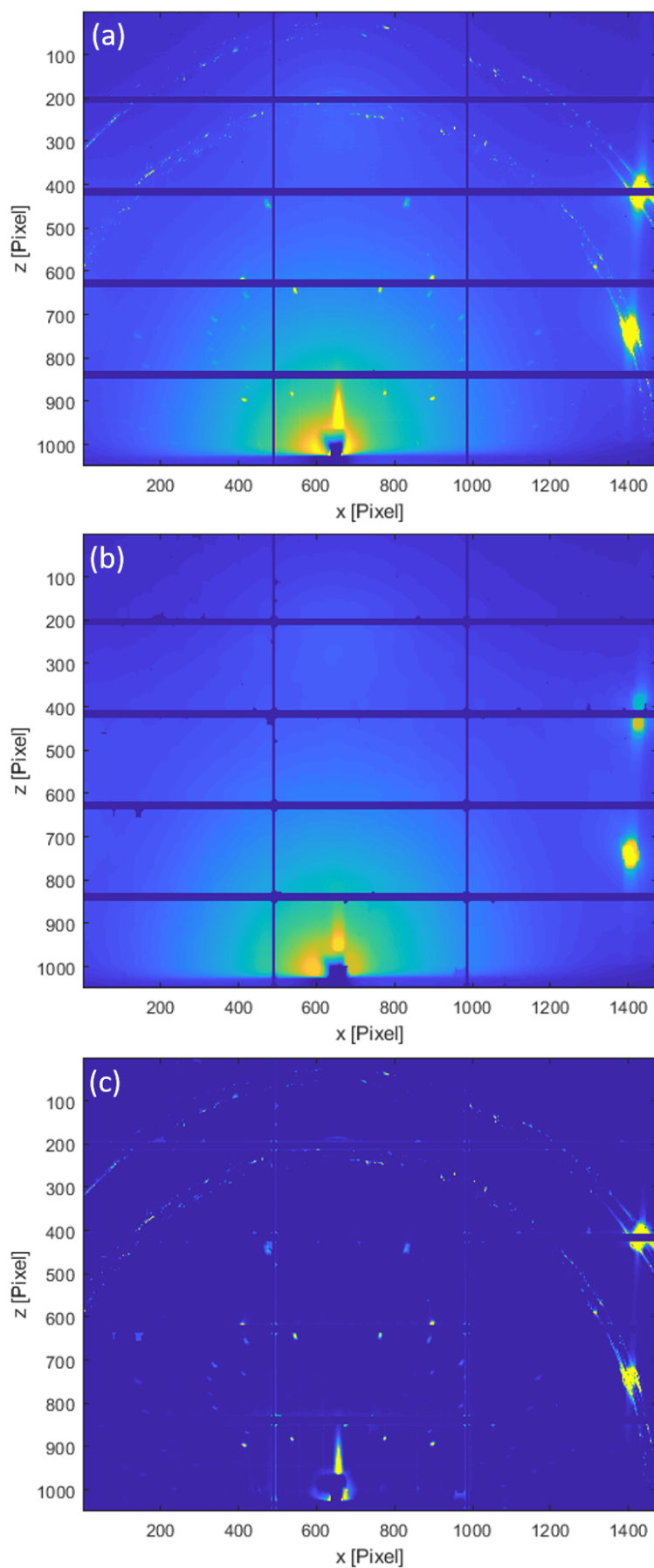
Figure 3.3: This series of figures show data of background correction of the diffraction data. (a) Diffraction pattern of Pentacenequinone on a Ag(111) surface originally measured at the detector. (b) The estimated background of the diffraction pattern of (a). Radius of disc size: 14 pixel. (c) The intensity difference between the original data (a) and estimated background(b).

3.2 Automatic search

3.2.1 Mark untrusted areas

Before the search procedure can start, untrusted areas have to be excluded. The untrusted areas of the detector are already marked after initialization. But there are also areas which are not interesting from an experimental point of view. The areas of the usually well known substrate peaks or the air scattering around the beamstop. There are three possibilities to ignore such areas, which will be discussed in the following section. An example of untrusted areas is shown in Figure 3.4.

Annulus

An annulus is an area between two concentric circles. This area can be marked by the user with an easy graphical input. After clicking on the button 'untrusted area annulus', a new figure opens. In this figure the user can click on a spot to mark the position of the middle circle of the annulus. In a subsequent step the user is asked to mark either the inner or the outer circle. The middle point of the annulus is the centre pixel. All pixels inside the annulus will be ignored during the search procedure. The area is marked in the GIXD data plot, by drawing the edges.

Box

A box is an area with an rectangular boarder. To create one of this boxes the button 'untrusted area Box' can be used. The position of the box can be easily marked by two clicks marking two diagonal points. The area is marked in the GIXD data plot, by drawing lines around the edges.

Freehand

A Further feature is the button 'untrusted area freehand', with an area which can be marked with a freehand drawn polygon.This areas are drawn with the following procedure: At first the left mouse button is pressed and then the mouse is dragged around the untrusted area. After releasing the mouse button, a straight line to the beginning of the free hand drawing will be created. Then the edges of this area will be marked in the main GIXD data frame.
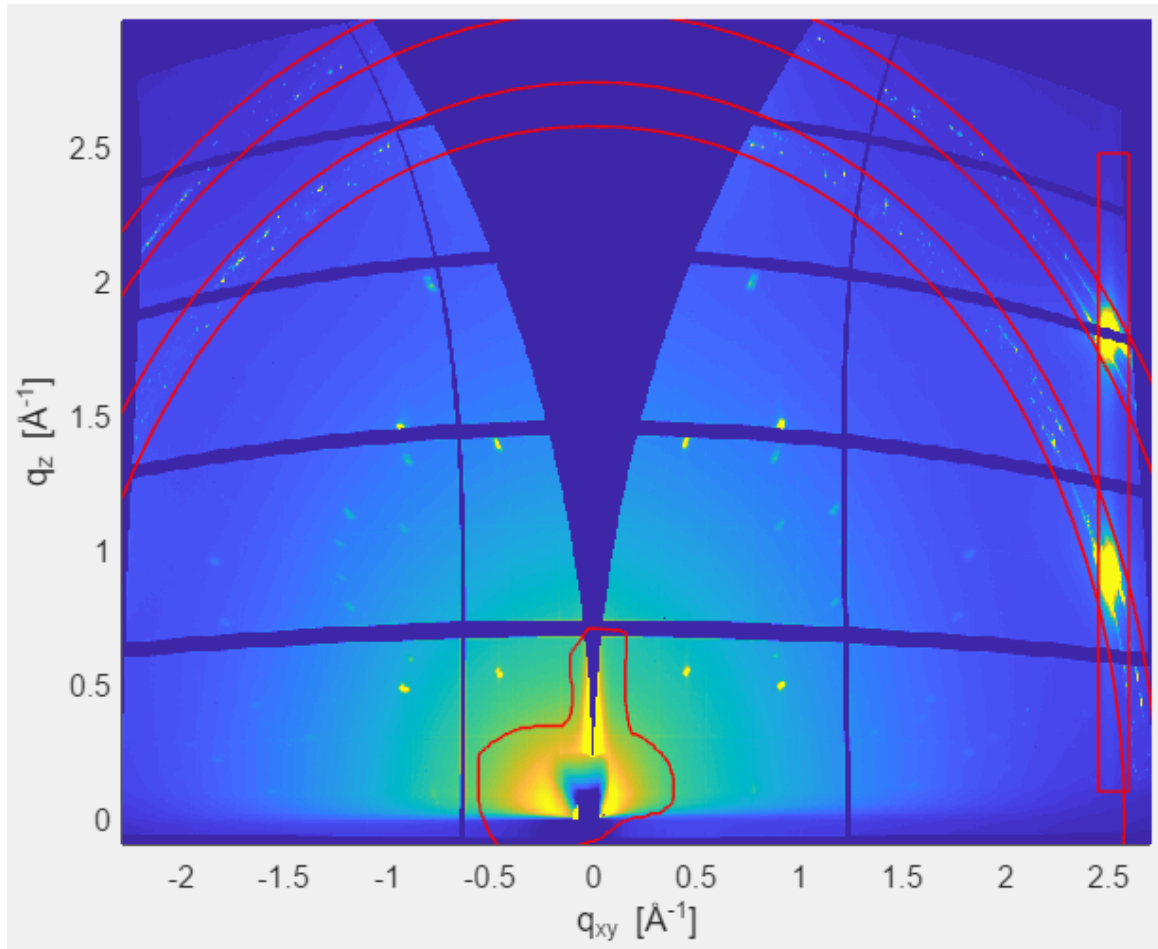
Figure 3.4: Different possibilities of untrusted areas: annulus (top), box (right) and freehand drawing(bottom)

3.2.2 Search procedure

Now the following question arises: How can a diffraction peak be defined? X-ray peaks follow roughly 2D Gaussian distribution for GIXD pattern. The aim of the search algorithm is drawing boxes around the peaks. At first the points of possible peaks have to be found. A point is only found when the following conditions are met:

- a local maximum

- not in a untrusted region

- equation 3.1 has to be fulfilled

The search algorithm looks at each pixel of the intensity map of the original diffraction data. When all of the conditions mentioned above are met, a box is drawn. This box has the identified point in the centre.

$$I_{experiment} - I_{Background} \geq \sqrt{I_{Background}} * U \qquad (3.1)$$

were: $I_{experiment}$......Intensity of GIXD data in counts
$I_{Background}$......Intensity of background data in counts
U.................user defined variable
$\sqrt{I_{Background}}$...noise of the diffraction background

The noise of the diffraction background is approximated with $\sqrt{I_{Background}}$, because the diffraction experiments follow a Poisson distribution. For this distribution, the variance is the mean value and standard deviation is the square root of the mean values[1]. Please note that $\sqrt{I_{Background}}$ is the mean value of the surrounding area(see section 3.1.1).
An important notion is that the intensity of the U value depends strongly on the experiment. With longer exposure time a more favourable peak to background ratio is generated. So, to reach the optimal search parameters the measurement time has to be as long as possible.

The next step of the search process is to merge the found boxes, if they overlap to get bigger smeared out peaks in only one box. Therefore during the merge step the biggest possible box will be created. There are four possibilities for box locations relation to one another:

1. the boxes do not touch each other

2. at least one edge of a box is in another other box

3. one box goes through an other box

4. one box is with all 4 corners in a other box
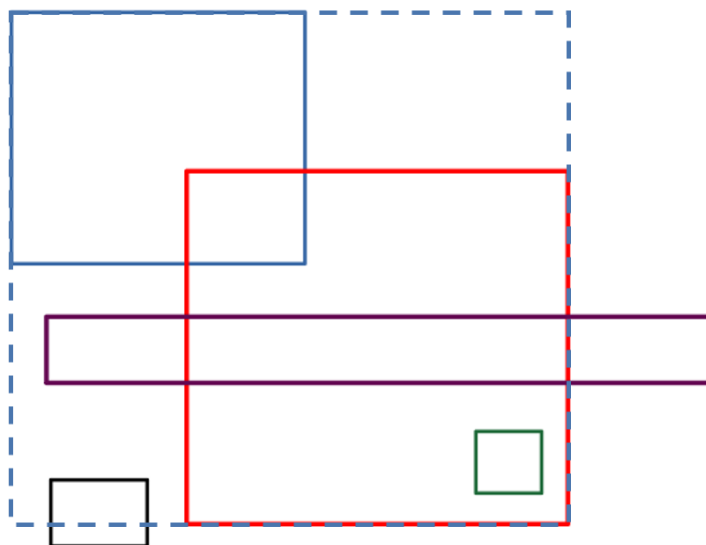
Figure 3.5: Possible locations of the boxes. The black box is located fully outside, thus is not merged. The green box is fully in the red box. The violet box transverses the red box. The blue box (full line) has only an overlay with one corner in the red box. The blue line (dashed line) is the merged box of the blue (full line) and red box.

An example of the boxes is shown in 3.5. The black and the red box will not merge. The green box is totally absorbed by the red box. The blue box is only by one corner in the red box, therefore the biggest possible box will be created. The violet box transverses the red box, and forms the biggest possible box. The merging algorithm is applied multiple times, so that the biggest possible boxes can be found. During these merging steps, a box can only merge once to avoid problems when three boxes overlap. After the merging of the first two boxes, the third is merged with the big box. In Figure 3.8, the merged boxes are displayed in the plotting area of the GUI. This Figure shows quite a lot boxes. The question arises: How many of these boxes are really boxes? The answer will be given in section 3.3.

Influence of U Value

It is possible to influence the outcome of the search procedure by changing the value of U. A higher U value will allow to find peaks with higher intensities and hence fewer boxes. This is shown in Figure 3.6, where the number of boxes has been plotted depending on their U Value. The low number of boxes at the beginning (U < 20) occurs, because all the boxes are in such close proximity, that they merge into a few big boxes. Important for this merging process is that this works iteratively. After a first step, were boxes merge, it is again checked, if any boxes could merge. If this is the case, they are merged again. This happens in the first range of U values until only one or a few other boxes are created. In the next range of U values(U $\geq$ 20), many non-overlapping peaks are identified. Most of these created boxes are usually false positives. When the range of the U Values is increased further on a "saturation" occurs. The "saturation" at the end happens, because at the end only very strong peaks are found. These peaks are found across very long ranges. Under consideration of all these effects the ideal U value is between the peak and the beginning of the saturation (U=60).
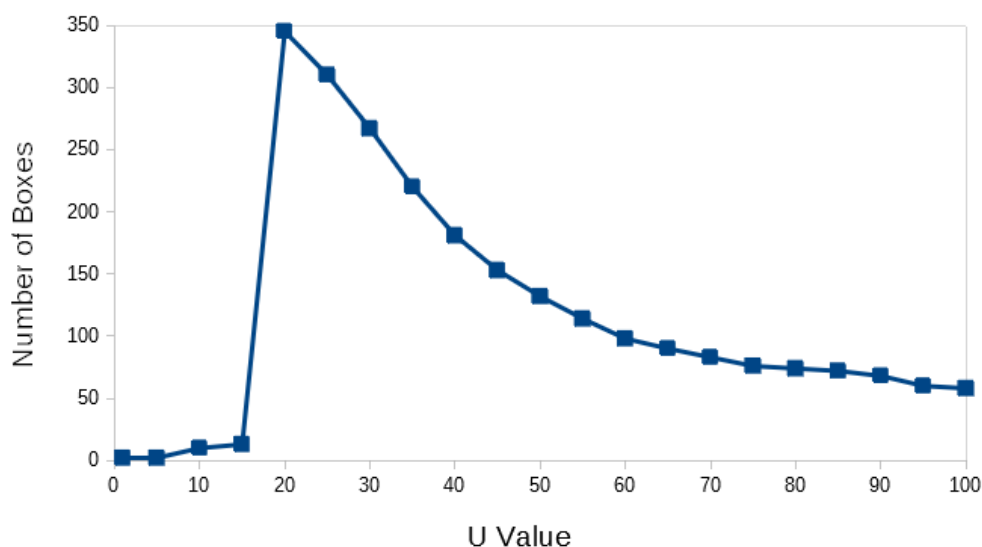

Figure 3.6: Number of Boxes depending on the U value.

However, tests with different strategies to find the U value have shown that a varying, the U value could be beneficial for the search of thin film peaks. These varying U values are dependent on the intensity values of the background. The U value changes in steps between two defined values. It can be defined how many steps are used. The background is split into intensity ranges. The number of these ranges is the same as the number of steps of U. The lowest background values corresponds to the U value given in the "Sensitivity end" field. The highest background value corresponds to the U value given in the "Sensitivity start" field. Hence, a specific U Value can be determined for each pixel depending on its estimated background. A sketch of this can be seen in Figure 3.7.
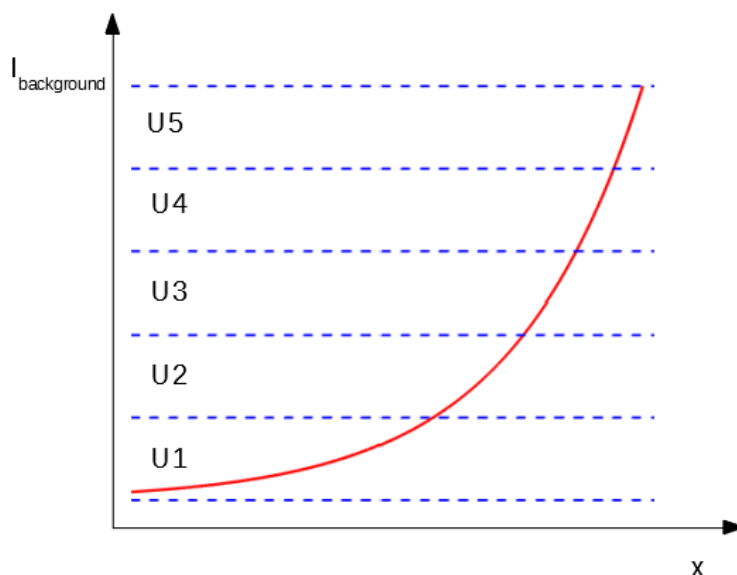
Figure 3.7: A diagram to illustrate the dependency of the U value on the background better. The red line symbolises the changing background intensity. The blue dashed line symbolise the edges of the range intervals. U1 ='Sensitivity start'; U5='Sensitivity end'; 'Sensitivity Steps'. I = the intensity of the estimated background; x = any direction, in which the background intensity changes
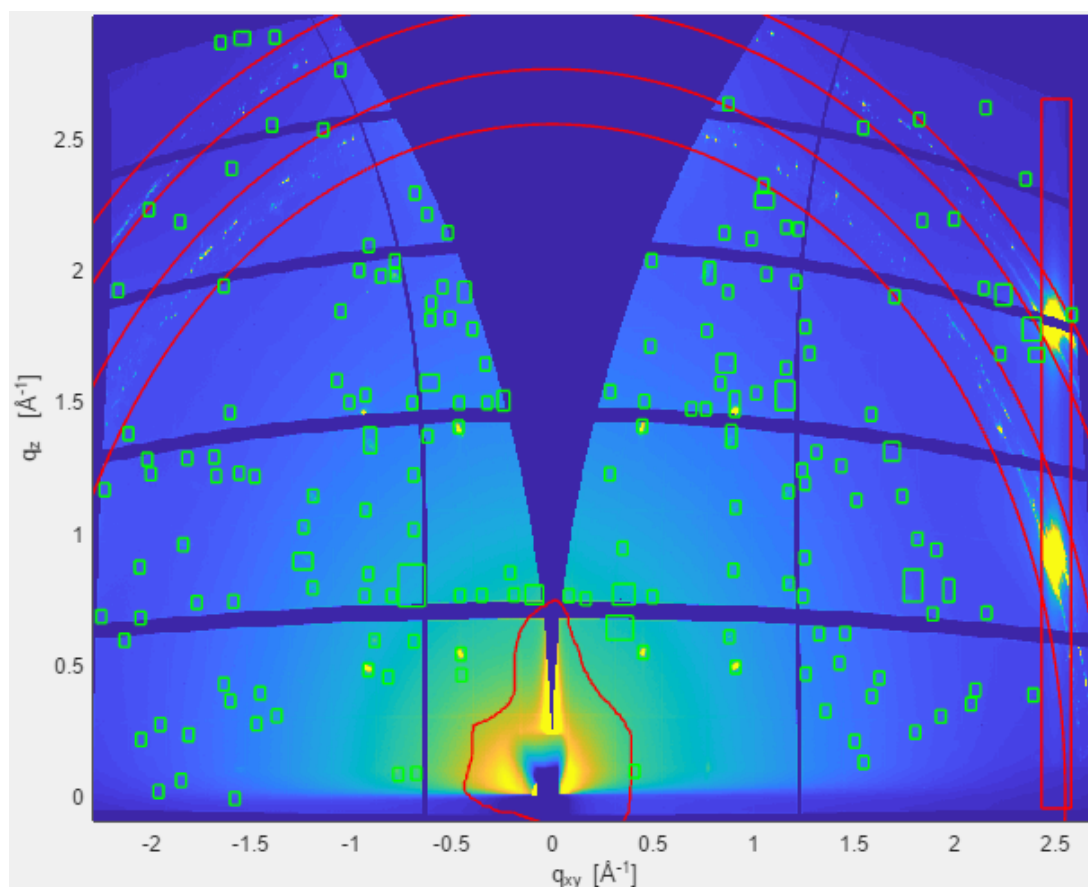
Figure 3.8: Successfully found boxes of the diffraction pattern. The following parameters are used to find these boxes: height= 0.05 Å^{-1}, width=0.05 Å^{-1}, U_{max}=40, U_{steps}=50, U_{min}=30.

3.3 Treatment of false positives

In this thesis a false positive is defined: A found box by the algorithm, where no peak is actually located. To find out if a box is a false positive or not, a criterion has to be taken into account. A good approximation for peaks of GIXD data is a two dimensional Gaussian peak. So for each of these boxes a Gaussian fit is performed. The maximum of this Gaussian fit is considered the peak position. If this fitted peak position is outside the box, the box is considered a false positive. The result of this procedure is shown in Figure 3.9. In this figure, the final stage of the processing of false positives (e.g. the box at $q_{xy} \sim 0.5$ Å^{-1} and $q_z \sim 0.5$ Å^{-1}) is shown. Please take care that sometimes the fit can strongly depend on area of box. Sometimes the boxes have to be manipulated so that strong peaks are recognised as peaks. This happens often in the regions of the edges of the detector panels. Also overlapping peaks (see section 3.3.1) may happen. To cover these cases, manual manipulations of the boxes and a new fitting step can be applied.
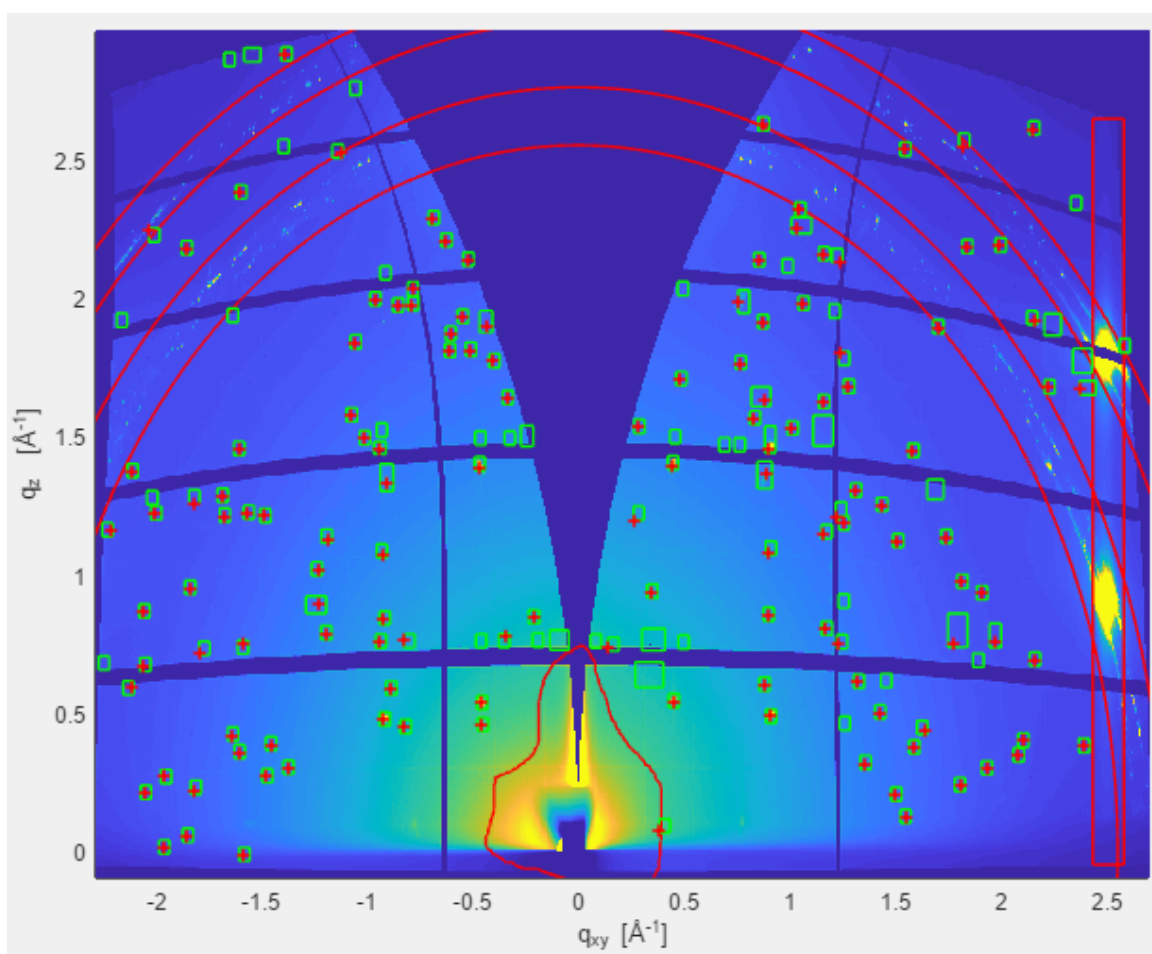

Figure 3.9: The plot after the 2 dimensional Gaussian fit to filter out false positives. The false positive boxes are still drawn. The green rectangles are the boxes and the red crosses are maxima of the Gaussian fit.

3.3.1 Manual manipulation

If the treatment of the false positives is not sufficient, the user can try to adjust the outcome by several manual manipulation possibilities for the boxes and thus the points for the Gaussian fit.

**Examples in which manual manipulation is required**

Before discussing the possibilities of manual manipulation two examples, in which the search algorithm has problems, are shown. The first problem can occur, when peaks are very close to each other. If the initial box size is to big, the peaks will merge as discussed above. An example of this is shown in Figure 3.10. To prevent the boxes from merging, there are two possibilities. The first is to adjust the initial box size so that the boxes do not merge. The second one is to simply delete the box which is to big and draw two smaller ones by hand.
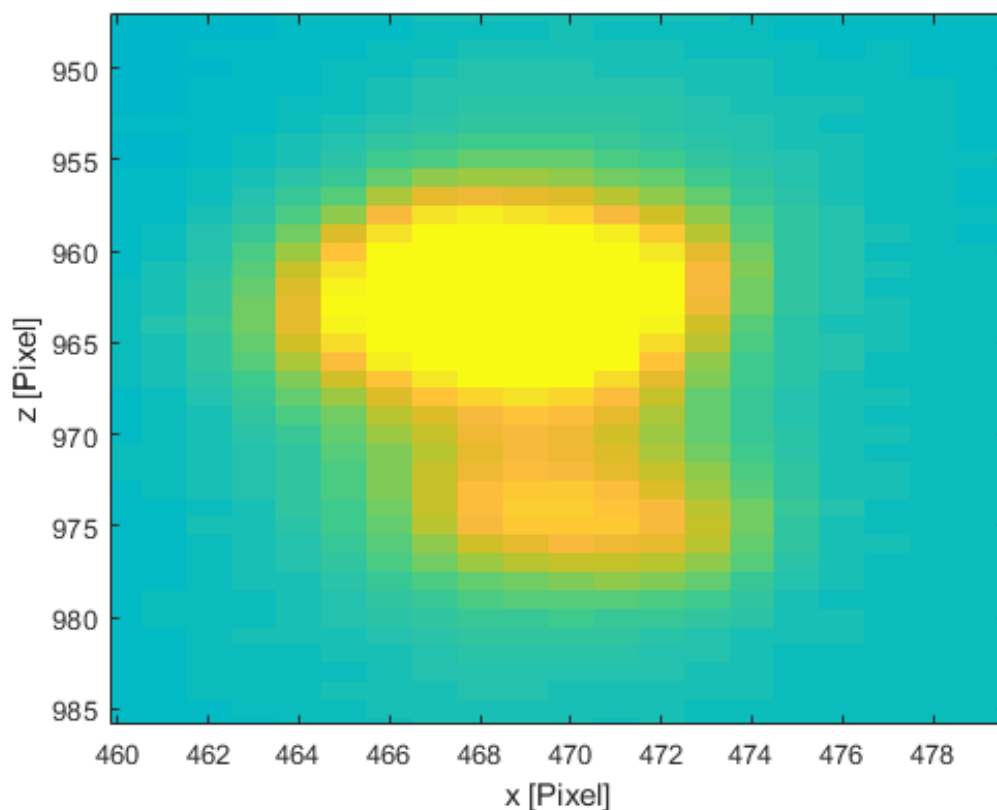
Figure 3.10: Two diffraction peaks located in close proximity to each other are shown. First peak: x= 465-473 pixel and z= 958-969 pixel. Second peak: x= 468-472 pixels and z=973-976 pixel

The second example is shown in Figure 3.11. Here, a diffraction peak is located in an untrusted area of the detector (higher intensity in detector panel x=860 pixel). This peak would never have be found by the search algorithm. Therefore, it needs to be added manually by drawing a box around it.
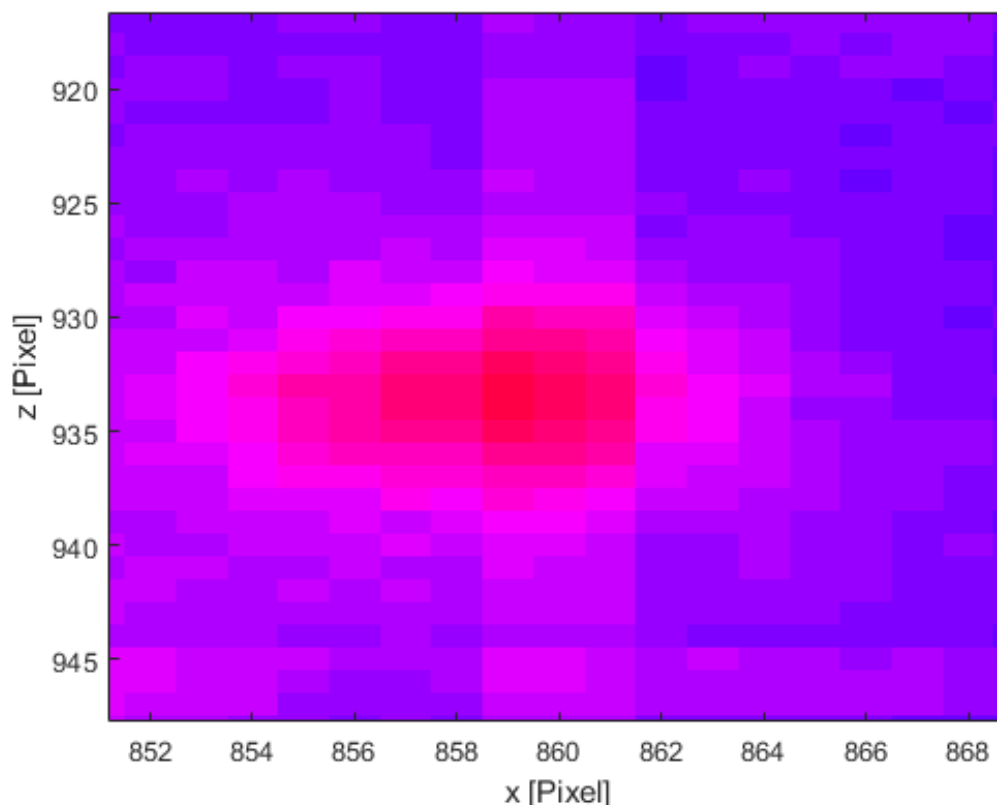
Figure 3.11: A peak located in untrusted area(x=860 pixel).

Drawing a Box

The first option is to draw additional boxes in the case in which the finding algorithm does not find all boxes. A good idea is to search in areas far away form the air scattering for very low peaks. This is usually the region where the peaks are so weak above the background that manual adding is necessary. If the user wants to draw a box they have to click the button 'Add box'. Then the procedure is identical to adding a box in untrusted areas.

Deleting Boxes

By clicking the button 'Remove Boxes', boxes can be removed with a line drawn by hand. Drawing this line works like the freehand option of untrusted area. All the boxes, which are with all four corners inside the line, will be removed. This option of allows to remove multiple boxes at once.

Merging Boxes

The 'Merge' button starts the merging algorithm discussed in section 3.2.2.

After the manual manipulation, the fit should be redone to check if better results are found. If they are acceptable, the user can either save this static GIXD data as a .txt file or go on with the next steps for rotating GIXD data. The following paragraph only treats data from static

GIXD. For information on how rotating GIXD data is proceeded, see section 3.4.

The saved data file consists of two columns, one for q_{xy} and one for q_z. Before the file is created the user can eliminate fits that have a bad fit. For this the user can define the goodness of fit. For the goodness of fit is the 'Root Mean Square Error' use. For 'Root Mean Square Error' the perfect fit would be 1 and the worst fit would be 0. For further information on 'Root Mean Square Error' see [17]. The user can also define what the minimum threshold of the σ value (the width) of the 2-dimensional Gaussian fit is in each direction. The remaining values can be shown with the button 'Show points'. The values are then saved by clicking the 'Save Fit Points' button, as q_{xy} and q_z in the file. The units of these points is 1/Å.

3.4 Rotating GIXD data

Up to this point, only the peaks of the 'Summed Image' or 'Maximum Intensity Image' are defined. So at this point it is not clear in which diffraction pattern of the rotation the peaks are actually located. To find these peaks, firstly a 'Multiple Scan plot' is created for each box. Then a two-dimensional Gaussian fit is performed in that picture. Finally, the q_{xy} position is split into its components q_x and q_y.

Before this procedure can start, all of the pictures of the rotation have to be loaded by clicking 'Load pictures'. Then a user interface similar to the one for inserting the 'beamtime file', is opened. In this interface multiple datasets can be selected.

3.4.1 Multiple Scan plot

Figure 3.12 shows two examples of two different multiple scan plots. See section 2.5.1 for information on how to create such figures. In Figure 3.12, a real peak and a peak, which is a false positive are depicted. In Subfigure 3.12a no clear peaks can be found. The peak shown is considered a false positive. In comparison to the accepted peaks, of Figure 3.12a the background is higher, but the peaks are not that stronger. The dashed magenta line is an estimated background. Here, the estimation of the background is a flat line located in the middle of the mean and the mode of the blue line. This combination has proven to obtain a good estimation of the background. In Figure 3.12b, there is an example of a peak in the box. The intensity of the peaks is much higher than the background. The maximum positions of these peaks are fitted with a one dimensional Gaussian fit. This fit is used to filter out some peaks, which are too broad, and also possible hot pixels. If a peak is accepted as a peak is determined by the following conditions:

- a local maximum

- equation 3.1 has to be fulfilled

The U value of this fit has to be inserted by the user. The name of the value is 'Sensitivity'. If the conditions are met, the highest point is taken and marked with a red circle. This process is started by clicking 'Find Pictures to Peak'. For each box a new figure, containing the 'Multiple Scan Image', is be opened. After inspecting of this figure, it can be closed by clicking the 'Close figures' button. It is also important to mention that in 3.12b there are 12 peaks.

(a)

(b)
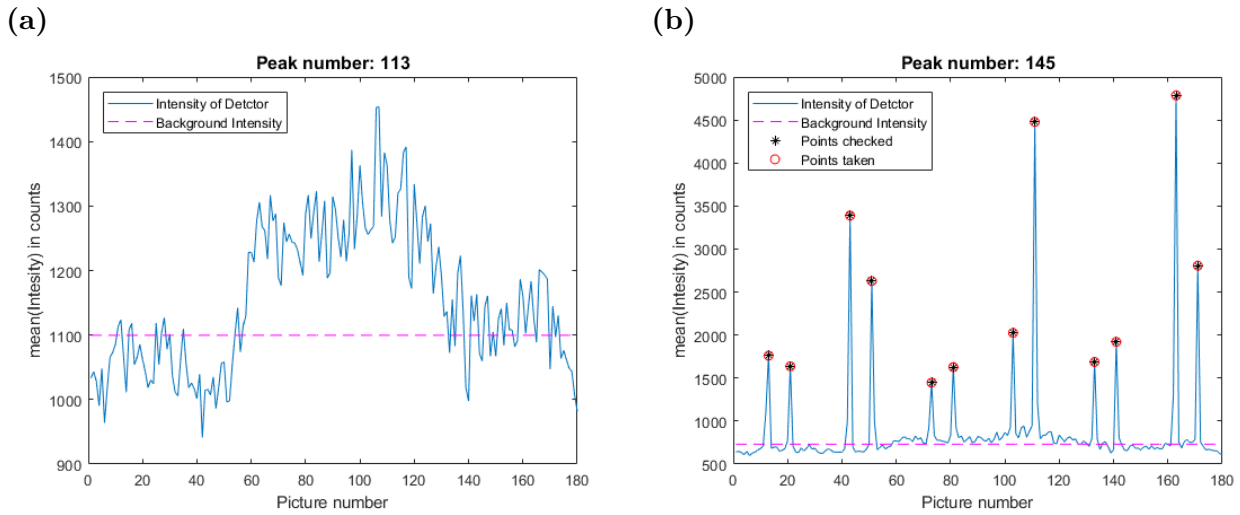
Figure 3.12: (a) Example of a multiple scan is which no peaks are taken located. This GIXD-peak is located in Figure 3.9 at $q_{xy} = -0.7$ Å^{-1} and $q_z = 1$ Å^{-1}.
(b) Example of a multiple scan were some points are taken. This GIXD-peak is located in Figure 3.9 at $q_{xy} = 0.9$ Å^{-1} and $q_z = 1.3 - 1.4$ Å^{-1}.
The blue line is the intensity found in the boxes in each diffraction pattern of the rotation. The dashed magenta line is an estimated background. The black stars mark points which are tested to be real peaks. The red circles are selected peaks. The rotation steps ($\Delta\phi$) equal 2°.

3.4.2 Treatment of peaks in individual ration image

For the accepted point, a two-dimensional Gaussian fit is redone in their respective pictures, because spots can differ from diffraction pattern to diffraction pattern. The maxima of these fits are again used as the position of the peaks. The peaks now have a known q_{xy} and q_z value and a known degree of rotation. The degree of rotation is determined by the number of the respective pictures. Also, a correction of the rotation value has to be applied. This is the case because a flat detector can not measure the whole area of a sphere. So the detector measures multiple Ewald spheres at once. This correction is numerical and is subtracted from the degree of rotation. Then the split of the q_{xy} positions happens. The relation of q_x, q_y and q_{xy} is a similar to polar space. So, following formulas are valid:

$$q_{xy} = \sqrt{q_x^2 + q_y^2} \tag{3.2a}$$

$$\phi = \arctan \frac{q_y}{q_x} \tag{3.2b}$$

$$q_x = q_{xy} * \sin \phi \tag{3.2c}$$

$$q_y = q_{xy} * \cos \phi \tag{3.2d}$$

3.4.3 Representation of data

The newly calculated three-dimensional scattering vector $\vec{q}$ is displayed as 3 dimension points. An example of this is Figure 3.13b. In this figure, the points are marked a red circles. A second option is a projection of this plot. One of the projections is the top view (q_x versus q_y). This projection can be seen in Figure 3.13c. In this picture, the six-fold rotation can clearly be seen. The GUI also allows q_x versus q_z and q_y versus q_z. Then, by using equation 3.2a, the data can be recalculated to show how good the calculated vector tips fit the GIXD data. This can be seen in Figure 3.13a. For this, it is important to note that the left and the right hand of the detector is always measuring the same data at different rotation angles, so the data is somewhat symmetric. If a peak occurs on the left side of the detector, it should, after a 180° rotation of the sample, be visible on the detectors right side. Both peaks are equally distanced from a symmetry axis. The symmetry axis is the $q_{xy} = 0$ Å^{-1} line. This relation is not used to find peaks, because this line is not in the middle of the detector. So if peaks occur in a detector gap, they are measured at the other side of the detector. Therefore symmetric comparison would be very hard to realize. A second reason is that if the sample is somewhat tilted during the experiment, this tilt is of course also shown on the detector and would needed to be corrected. The peak finding algorithm of *APF* also has the big advantage, that it works with the original data. In Figure 3.13a the green boxes are the found boxes, and the red circles are the accepted peaks. In this case it is very obvious that a lot of the possible points are filtered out during the "Multiple Scan plot" and the two dimensional Gaussian fit comparison with the user-given thresholds can be filtered out. As described at the end of the static GIXD section, the result can be saved as a .txt file. Also, a threshold for the goodness of fit and the sigma values of the fit can be set. The printed data is q_x,q_y and q_z. The unit is again Å^{-1}.
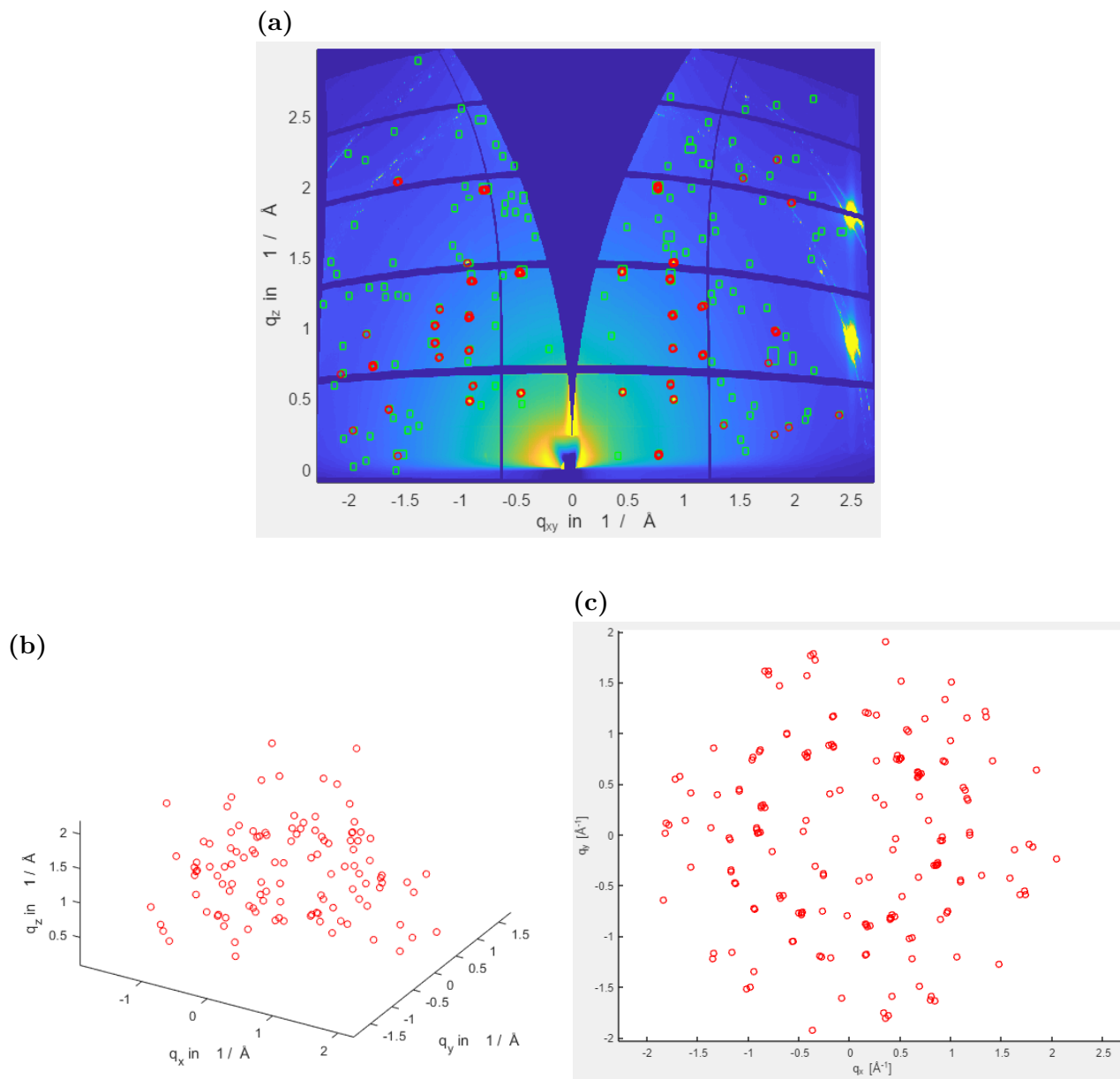
Figure 3.13: (a) The measured GIXD map with the calculated points of the scattering vector $\vec{q}$. The green boxes are the found boxes, and the red circles are the accepted peaks. (b) A - dimensional plot of the endpoints of the scattering vector $\vec{q}$. (c) The $\vec{q_x}$ versus $\vec{q_y}$ positions of the scattering vector $\vec{q}$.

4 Examples

In this chapter several examples are discussed to show the effectiveness of the algorithm of the *Automatic Peak Finder*. These examples are two epitaxial grown layers and one single crystal on a silicone substrate. During these evaluations the possibility of manual corrections was not used, to show the effectiveness of the algorithm.

4.1 Pentacenequinone

Comparison with single crystal software

As a first example, a Pentacenequinone sample has been searched by a single crystal software called XDS [6] and then compared to points found with the Automatic Peak Finder. This example is shown in Figure 4.1. In this figure it can be seen clearly that some points close to $q_{xy} = 0$ Å^{-1} are only found by XDS. These points are located in a untrusted zone of the automatic peak finding algorithm. Then, there are also some points at $q_{xy} = 2.5$ Å^{-1} and $q_z = 0.75$ Å^{-1}. These points are also located in an untrusted area of an smeared out substrate peak. The *Automatic Peak Finder* is very sensitive in this example, so numerous points of a very small powder-like ring with the radius of approximately 1.5 Å^{-1} are found. The algorithm of XDS which is designed to find single crystal peaks has problems to find the same amount of thin film peaks, like the algorithm of *Automatic Peak Finder*.
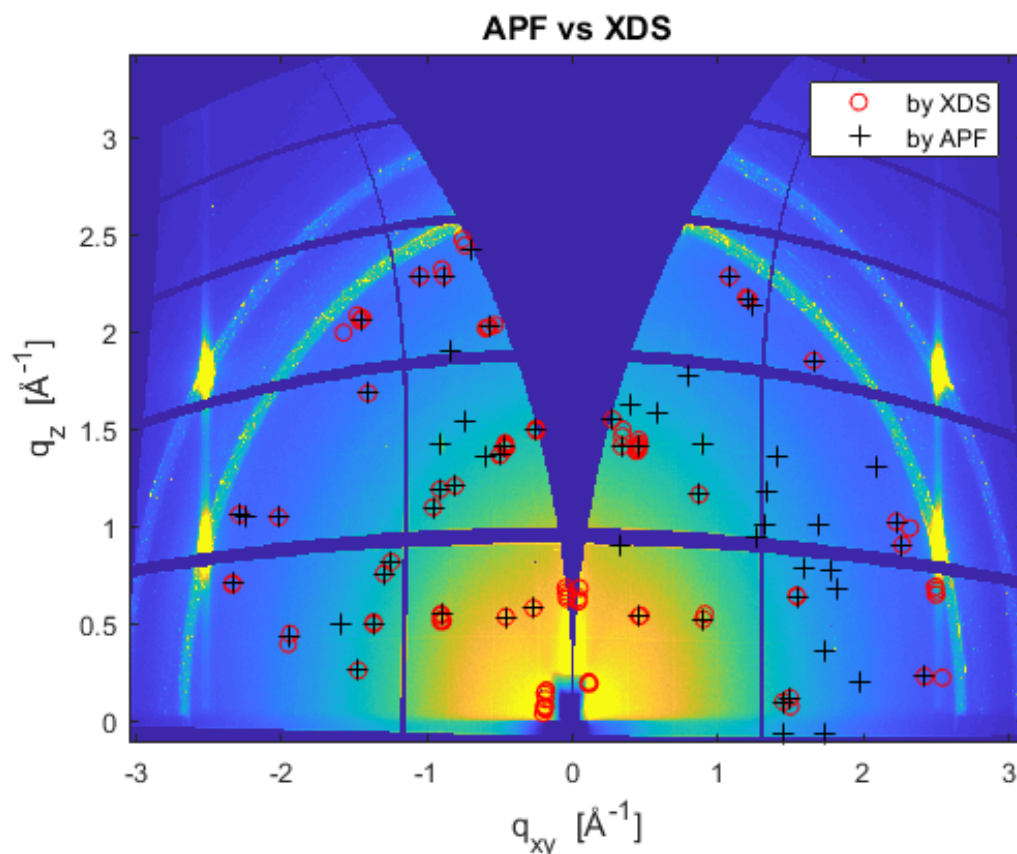
Figure 4.1: Comparison of a single crystal evaluation software XDS(red circles) with APF(black crosses) of Pentacenequinone on a Ag(111).

Manual comparison

In this section, another measurement of the Pentacenequinone is compared to an manual search. This can be seen in Figure 4.2. The red circles are the points found manually, the black crosses are found by the algorithm of the Automatic Peak Finder. The manual search has found 55 separate peaks. Of these peaks, 33 are found by APF. That is a ratio of 60 percent. There are also some points which are only manually found. The majority of the not found peaks are very weak above the background and thus not found. These peaks are usually located in the outer regions of the data (q_{xy} lower than -1.5 Å^{-1} and bigger than 1.5 Å^{-1}). There are also some false positives still in the data ranging at very low q_z positions and around $q_{xy} = 1.25$ Å^{-1} to 1.5 Å^{-1}. An important notion is that it is not that much of a problem that the point at $q_{xy} =$ -0.5 Å^{-1} and q_z around 1.4 Å^{-1} is not found, because the symmetrical peak at $q_{xy} = 0.5$ Å^{-1} is found instead. The opposite case can also be seen in this figure. The peaks at around $q_{xy} = -1$ and $q_{xy} = 1$ and a q_z value of 1.4 Å^{-1} are found more consistent than by the manual search. It is also important to mention that these peaks at the detector panel edges are somewhat hard to fit. For these points, manual manipulation can improve the quality of the search considerably, but as mentioned above, this does not apply to these examples.
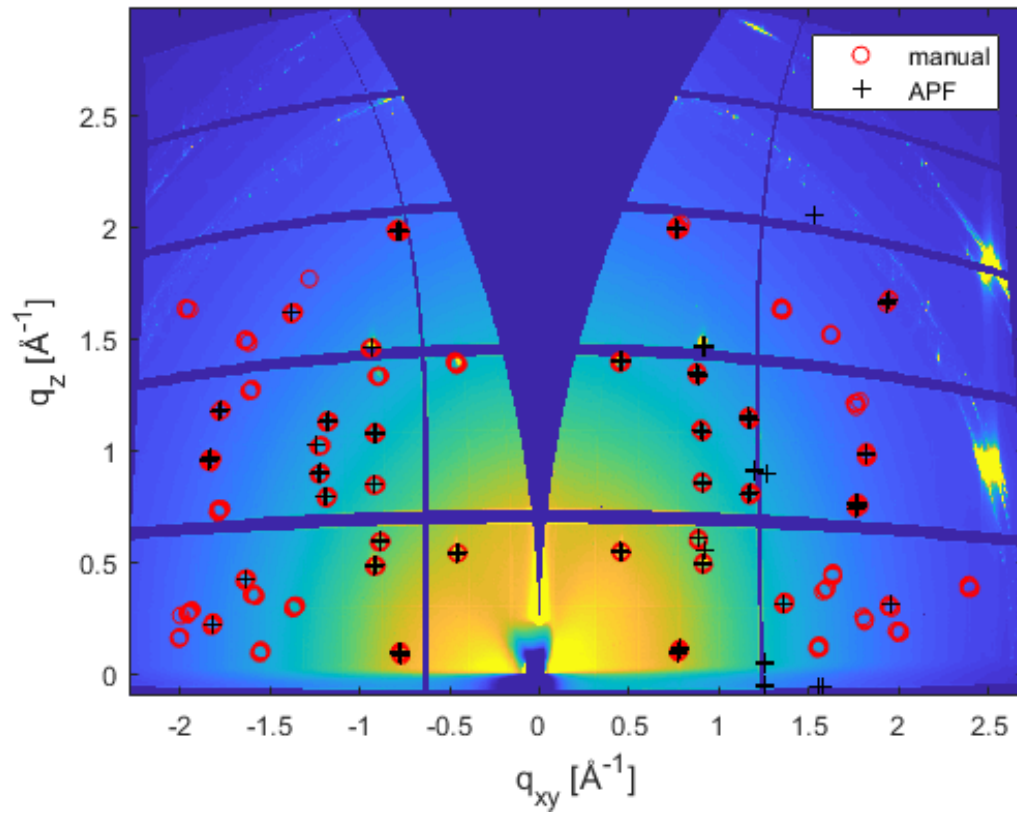
Figure 4.2: Comparison of a manual search (red circles)[14] to points found by *APF* (black crosses) of Pentacenequinone on a Ag(111).

4.2 Sexithiophene on Potassium-chloride

This is an example of a more difficult case. As Figure 4.3 shows, there are a considerable amount of untrusted areas. In these areas, there are a lot of Debye-Scherrer ring-like structures. This means that the search area near some points may be close to the untrusted areas.
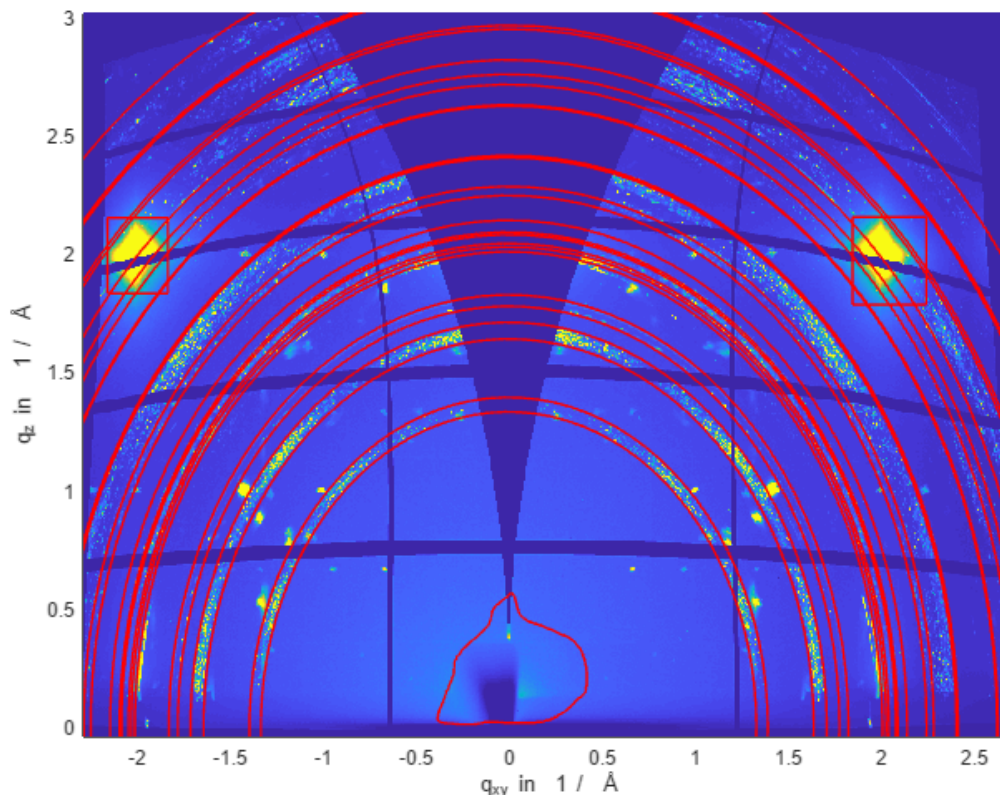
Figure 4.3: A maximum intensity picture of Sexithiophene peaks on a KCL substrate. This example shows that there are many Debye-Scherrer like areas, which are untrusted.

This example is also compared to manual[13] searched data shown as red circles in Figure 4.4. The points found by the peak finder algorithm are marked as black crosses. The figure clearly shows that nearly all of manual found peaks are also found by the algorithm. Some manually found points are located in the untrusted zones and thus are not found. There are also some weak points considered peaks by the manual search (located at $q_{xy} = 1.3$ Å^{-1} and q_z between 1 Å^{-1} and 1.5 Å^{-1}). All in all, this example shows that the peak search does very well although many areas are untrusted, because of the materials powdery behaviour.
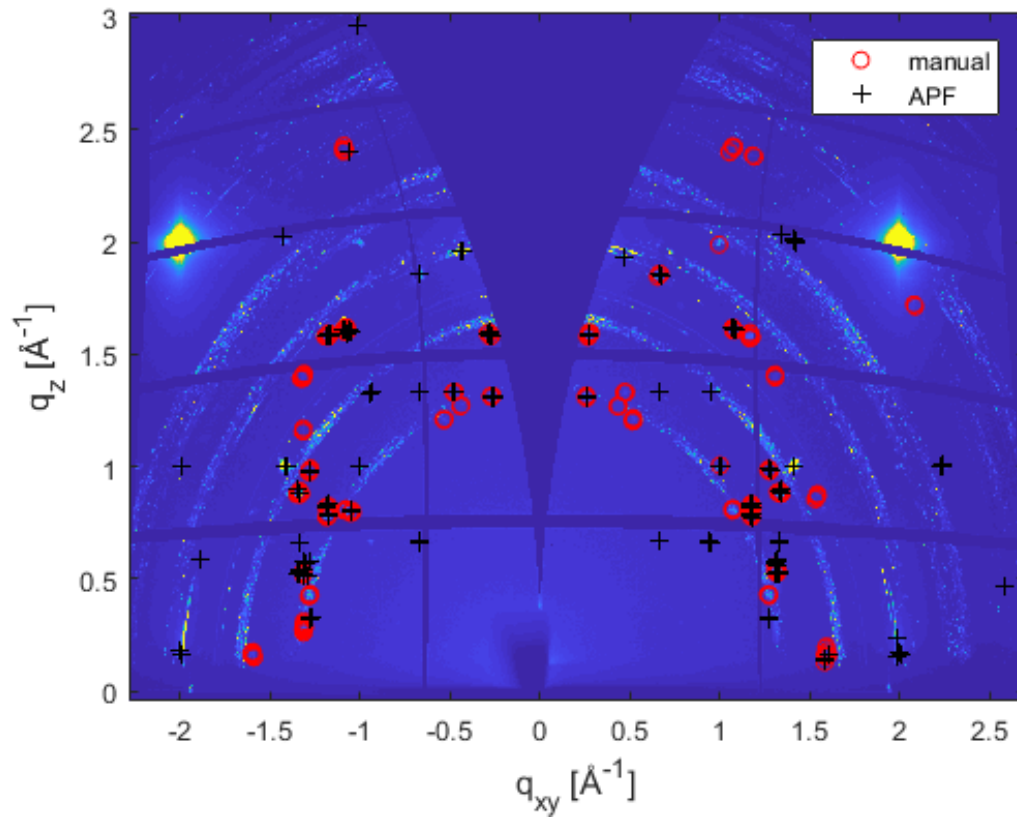
Figure 4.4: Comparison of a manual search[13] (red circles) to points found by *APF* (black crosses) of Sexithiophene on KCl.

4.3 Potassium hydrogenphthalate

This sample is a Potassium hydrogenphthalate (short: KAP) crystal in (010) orientation on a silicon substrate. The KAP structure is already known in literature [4].

In Figure 4.5 a summed image of a KAP crystal on a silicon oxide surface can be seen. This KAP crystal is put on a silicon oxide substrate. The silicon substrate has an adhesive layer transferred by a tape on it. In the figure it can be clearly seen that the peaks are smeared out in the "summed image". Most of the points are located around the theoretically expected points. An explanation is that the crystal is not well aligned with the substrate and thus wobbles around during the rotation measurement. This wobbling causes the peaks of the KAP crystal to move around their positions. The theoretical values are created with the GIDVis crystal module and literature data [4].
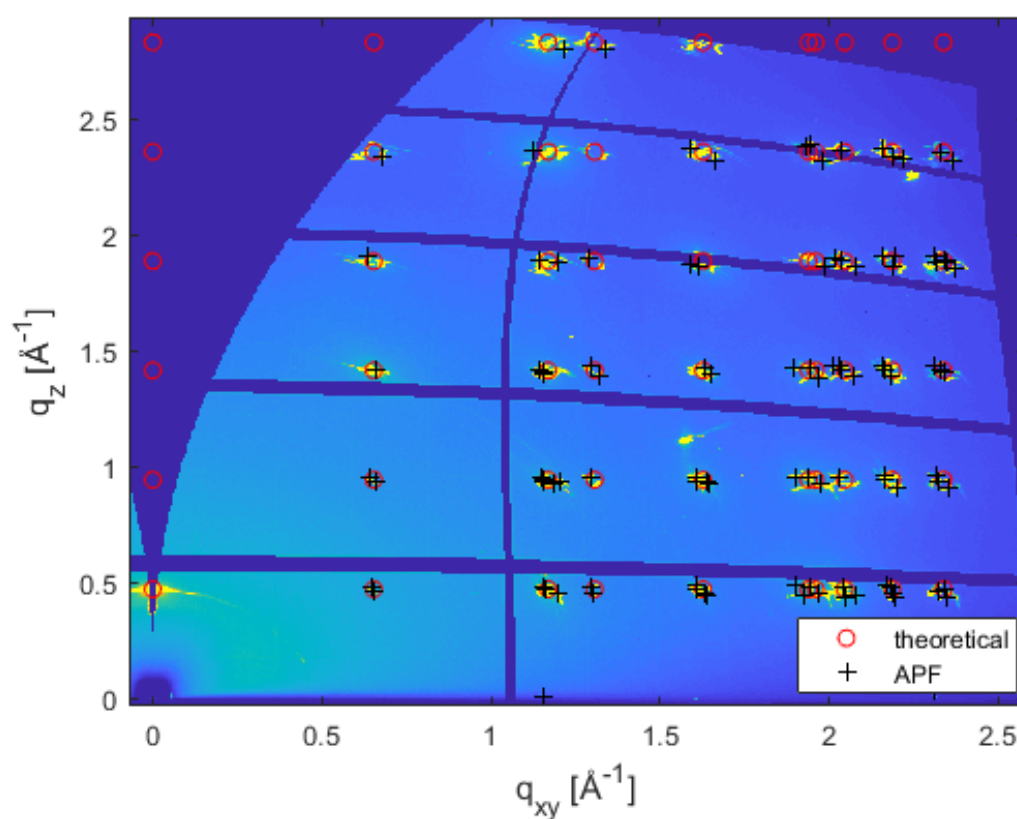
Figure 4.5: Comparison of theoretical data [4](red circles) to points found by **APF** (black crosses) of KAP on a silicon substrate.

5 Conclusion

The *Automatic Peak Finder (APF)* offers a graphical user interface to finds peaks in grazing incident diffraction patterns. Due to the fact that the *APF* is created as a part of GIDVis, some functions of GIDVis are reused. For example the same display options for diffraction patterns are used: "Q space" and "Polar space". A "beamtime file", which contains information of the measurement setup and is created by GIDVis is also needed for *APF*. The *Automatic Peak Finder (APF)* is a tool to support the finding diffraction peaks with several search steps, depending on the type of grazing incident X-ray diffraction (GIXD) measurement.

For static GIXD (see: section 2.1.1) at first some regions can be excluded. This exclusion can be caused by detector properties or unwanted features of the experiment. To ignore the unwanted features of the experiment (e.g. air scattering or substrate peaks) these regions can be ignored by three possibilities (see section: 3.2.1.): (i) drawing a box, (ii) drawing an annulus, (iii) making a freehand drawing. The next step in the workflow is to find possible peaks. To find these peaks they must be a local maximum; they must not lay in an untrusted area and must follow: $I_{experiment} - I_{Background} \geq \sqrt{I_{Background}} * U$. Around possible peaks a box with a defined initial size is drawn. If one or more of these boxes overlap, they merge to the biggest possible box. For the found boxes a two dimensional Gaussian fit is performed. The maxima of these fits are supposed to be peak positions. If the peaks are located outside of the box, the box is considered a false positive. If, because of any reason the area of the fits needs improvement, there are several possibilities for manual refinement of the boxes: (i) adding a box, (ii) deleting a box, (iii) merging the boxes. After the refinement step, the fit has to be performed again. For the output files, also threshold values for the half width of the fit and the goodness of the fit have to be defined. For rotating GIXD the q_{xy} component can be split into q_x and q_y. For this, the same procedure as for static GIXD has to be applied until the refinement is finished. Until this point a "Summed Image" or a "Maximum Image" (see section 2.5) is used. Then for each accepted box, it is possible to determine the degree of the rotation, in which peaks occur. With this information, it is possible to determine all three components of the scattering vector $\vec{q}$. After this determination, the scattering vector $\vec{q}$ can be saved as a "*.txt" file. Also, the thresholds of the fits can be applied.

To show the effectiveness of this algorithms several examples are discussed. For non of these examples the manual refinement was used. The first example compares the *Automatic Peak Finder* to the single crystal software XDS (see section 4.1) of an Pentacenequinone film on an silicon oxide sample. It is shown that not only all peaks are found by XDS (ignoring the peaks of air scattering, which are only found by XDS) are found by *APF*, but also weaker peaks are found by *APF*. For the same material peaks found by *APF* are also compared to manually found peaks. Here, around 50% of the peaks are found manually by the algorithm, but it has to be mentioned that most of these not found points are barely distinguishable from the background, by the eye. ANother comparison of peaks found by *APF* and a manual search has been conducted with Sexithiophene on potassium-chloride. Due to the fact that Potassium-chloride is polycrystalline, it is not easy to find some peaks in this example, but the algorithm of *Automatic Peak Finder* finds the same peaks as the manual search. Also, an interesting example is a measurement of potassium hydrogenphthalate. For this sample the orientation and the crystal structure already exist in literature. As it can be seen although the measurement is not ideal, all the theoretical peaks are found. It has to be mentioned that in this example, the sample seems to wobble around and so the peaks are also distributed around the theoretical points.

List of Figures

Bibliography

[1] Dennis W. Bennett. *Understanding Single-Crystal X-Ray Crystallography*. WILEY-VCH VerlagGmbH & Co. KGaA, 2010. ISBN: 978-3-527-32677-8 (HC), 978-3-527-32794-2(SC).

[2] Mario Birkholz. *Thin FIlm Analysis by X-Ray Scattering*. WILEY-VCH, 2006. ISBN: 978-3-527-31052-4.

[3] Jeff Dahl. *X-ray diffraction pattern 3clpro.jpg*. Wikimedia Commons. URL: https://en.wikipedia.org/wiki/File:X-ray_diffraction_pattern_3clpro.jpg.

[4] T.A. Eremina et al. "ABSOLUTE-CONFIGURATIONS AND CHARACTERISTICS OF MORPHOLOGY OF POTASSIUM BIPHTHALATE CRYSTAL". In: *Kristallografiya* 38 (1993), p. 236.

[5] Enrico Fumagalli et al. "Grazing-incidence X-ray diffraction study of rubrene epitaxial thin films". In: *Journal of Synchrotron Radiation* 19.5 (Sept. 2012), pp. 682–687. DOI: 10.1107/S0909049512027562. URL: https://doi.org/10.1107/S0909049512027562.

[6] Wolfgang Kabsch. "*XDS*". In: *Acta Crystallographica Section D* 66.2 (Feb. 2010), pp. 125–132. DOI: 10.1107/S0907444909047337. URL: https://doi.org/10.1107/S0907444909047337.

[7] Philipp Kraft. "PILATUS 2M. a detector for small angle X-ray scattering". en. Diss., Eidgenössische Technische Hochschule ETH Zürich, Nr. 18466, 2010. PhD thesis. Zürich: ETH Zurich, 2010. DOI: 10.3929/ethz-a-006023165.

[8] Christian Werner Röthel. *X-ray diffraction of organic thin films: crystalline texture in uniplanar systems*. eng. 2017.

[9] Elettra-Sincrotrone Trieste S.C.p.A. *Webpage: Spezification of XDR1 beamline @ Elettra*. Ed. by Elettra-Sincrotrone Trieste S.C.p.A. URL: https://www.elettra.trieste.it/lightsources/elettra/elettra-beamlines/xrd1/xrd1specifications/all.html.

[10] B. Schrode. *GIDVis - Guide and Tutorials*. May 2019. URL: https://www.if.tugraz.at/amd/GIDVis/.

[11] Benedikt Schrode. "From grazing incidence diffractionto pole figures and epitaxy". In: *Oberseminar TU Graz*. 2019.

[12] Benedikt Schrode et al. "*GIDVis*: a comprehensive software tool for geometry-independent grazing-incidence X-ray diffraction data analysis and pole-figure calculations". In: *Journal of Applied Crystallography* 52.3 (June 2019), pp. 683–689. DOI: 10.1107/S1600576719004485. URL: https://doi.org/10.1107/S1600576719004485.

[13] Günther Schwabegger et al. "Morphological and Structural Investigation of Sexithiophene Growth on KCl (100)". In: *Crystal Growth & Design* 13.2 (2013). PMID: 23413362, pp. 536–542. DOI: 10.1021/cg3010823. eprint: https://doi.org/10.1021/cg3010823. URL: https://doi.org/10.1021/cg3010823.

[14] J. Simbrunner et al. "An Efficient Method for Indexing Grazing-Incidence X-Ray Diffraction Data of Epitaxially Grown Thin Films." In: *Acta Crystallographica Section A Foundations and Advances (accepted)* (2019).

[15] Josef Simbrunner et al. "Indexing grazing-incidence X-ray diffraction patterns of thin films: lattices of higher symmetry". In: *Journal of Applied Crystallography* 52.2 (Apr. 2019), pp. 428–439. DOI: 10.1107/S1600576719003029. URL: https://doi.org/10.1107/S1600576719003029.

[16] Josef Simbrunner et al. "Indexing of grazing-incidence X-ray diffraction patterns: the case of fibre-textured thin films". In: *Acta Crystallographica Section A* 74.4 (July 2018), pp. 373–387. DOI: 10.1107/S2053273318006629. URL: https://doi.org/10.1107/S2053273318006629.

[17] Inc. The MathWorks. *Online Documentation of Matlab Help: Evaluating Goodness of Fit.* Ed. by The MathWorks, Inc. URL: https://de.mathworks.com/help/curvefit/evaluating-goodness-of-fit.html.

[18] Inc. The MathWorks. *Online Documentation of Matlab Help: imopen.* Ed. by The Math-Works, Inc. URL: https://de.mathworks.com/help/images/ref/imopen.html?searchHighlight=imopen%5C&s_tid=doc_srchtitle.

[19] Inc. The MathWorks. *Online Documentation of Matlab Help: uigetfile.* Ed. by The Math-Works, Inc. URL: https://de.mathworks.com/help/matlab/ref/uigetfile.html.